WTK-LED: The WIND Toolkit Long-Term Ensemble Dataset

Caroline Draxl,[1] Jiali Wang,[2] Lindsay Sheridan,[3] Chunyong Jung,[2] Nicola Bodini,[1] Sarah Buckhold,[4] Connor T. Aghili,[2] Kyle Peco,[2] Rao Kotamarthi,[2] Andrew Kumler,[1] Caleb Phillips,[1] Avi Purkayastha,[1] Ethan Young,[1] Evan Rosenlieb,[1] and Heidi Tinnesand[1]

1 National Renewable Energy Laboratory
2 Argonne National Laboratory
3 Pacific Northwest National Laboratory
4 University of Wyoming

NREL is a national laboratory of the U.S. Department of Energy
Office of Energy Efficiency & Renewable Energy
Operated by the Alliance for Sustainable Energy, LLC

This report is available at no cost from the National Renewable Energy Laboratory (NREL) at www.nrel.gov/publications.

Contract No. DE-AC36-08GO28308

Technical Report
NREL/TP-5000-88457
October 2024

WTK-LED: The WIND Toolkit Long-Term Ensemble Dataset

Caroline Draxl,[1] Jiali Wang,[2] Lindsay Sheridan,[3] Chunyong Jung,[2] Nicola Bodini,[1] Sarah Buckhold,[4] Connor T. Aghili,[2] Kyle Peco,[2] Rao Kotamarthi,[2] Andrew Kumler,[1] Caleb Phillips,[1] Avi Purkayastha,[1] Ethan Young,[1] Evan Rosenlieb,[1] and Heidi Tinnesand[1]

1 National Renewable Energy Laboratory
2 Argonne National Laboratory
3 Pacific Northwest National Laboratory
4 University of Wyoming

Suggested Citation
Draxl, Caroline, Jiali Wang, Lindsay Sheridan, Chunyong Jung, Nicola Bodini, Sarah Buckhold, Connor T. Aghili, et al. 2024. *WTK-LED: The WIND Toolkit Long-Term Ensemble Dataset*. Golden, CO: National Renewable Energy Laboratory. NREL/TP-5000-88457. https://www.nrel.gov/docs/fy25osti/88457.pdf.

NREL is a national laboratory of the U.S. Department of Energy
Office of Energy Efficiency & Renewable Energy
Operated by the Alliance for Sustainable Energy, LLC

This report is available at no cost from the National Renewable Energy Laboratory (NREL) at www.nrel.gov/publications.

Contract No. DE-AC36-08GO28308

Technical Report
NREL/TP-5000-88457
October 2024

National Renewable Energy Laboratory
15013 Denver West Parkway
Golden, CO 80401
303-275-3000 • www.nrel.gov

NOTICE

This work was authored in part by the National Renewable Energy Laboratory, operated by Alliance for Sustainable Energy, LLC, for the U.S. Department of Energy (DOE) under Contract No. DE-AC36-08GO28308. Funding provided by the U.S. Department of Energy Office of Energy Efficiency and Renewable Energy Wind Energy Technologies Office. The views expressed herein do not necessarily represent the views of the DOE or the U.S. Government.

Cover Photos by Dennis Schroeder: (clockwise, left to right) NREL 51934, NREL 45897, NREL 42160, NREL 45891, NREL 48097, NREL 46526.

Acknowledgments

The creation of the Wind Integration National Dataset (WIND) Toolkit Long-Term Ensemble Dataset (WTK-LED) would not have been possible without support from the DOE Wind Energy Technologies Office. The team is particularly grateful for Patrick Gilman's and Bret Barker's support over the years. Various teams and researchers across the National Renewable Energy Laboratory (NREL) contributed to the WTK-LED by either giving input in the design stage or using the data and thereby shaping the final version of the WTK-LED: Eric Lantz, Greg Brinkman, Trieu Mai, Cong Feng, Ryan King, Brandon Benton, Dmitry Duplyakin, and Zagi Zisman. We also thank the grid team at the Pacific Northwest National Laboratory for vetting the data for grid integration studies. We are grateful to the development team of the Wind Resource Database for providing an easy platform for data viewing and downloading: Rachel Barton, Paul Edwards, Jason Ferrier, Nick Gilroy, Amber Mohammad, Reid Olson, and Paul Susmarski.

The Weather Research and Forecasting model simulations and analyses were performed on the high-performance computing system Eagle at NREL, the high-performance computing system Cheyenne provided by the National Center for Atmospheric Research's Computational and Information Systems Laboratory, sponsored by the National Science Foundation (Computational and Information Systems Laboratory n.d.), and the high-performance computing system Theta provided by the Argonne Leadership Computing Facility.

List of Acronyms

CONUS	contiguous United States
ERA5	European Centre for Medium-Range Weather Forecasts Reanalysis version 5
HRRR	High-Resolution Rapid Refresh
HSDS	Highly Scalable Data System
km	kilometer
LSM	land surface model
m	meter
MAE	mean absolute error
MERRA	Modern-Era Retrospective analysis for Research and Applications
min	minute
MYNN	Mellor-Yamada-Nakanishi-Niino
NCAR	National Center for Atmospheric Research
NoahMP	Noah-Multiparameterization Land Surface Model
NOW-23	2023 National Offshore Wind [dataset]
NREL	National Renewable Energy Laboratory
PBL	planetary boundary layer
PDF	probability density function
RMSE	root-mean-square error
TKE	turbulence kinetic energy
UH	University of Hawaii
WIND Toolkit	Wind Integration National Dataset Toolkit
WRDB	Wind Resource Database
WRF	Weather Research and Forecasting [model]
WTK-LED	WIND Toolkit Long-term Ensemble Dataset
YSU	Yonsei University

Executive Summary

The updated version of the Wind Integration National Dataset (WIND) Toolkit (Draxl et al. 2015a)—named WIND Toolkit Long-term Ensemble Dataset (WTK-LED)—is a meteorological dataset that provides high-resolution time series, including interannual variability and model uncertainty of wind speed at every modeling grid point to indicate ranges of possible wind speeds. WTK-LED aims to close gaps in current public datasets to better serve stakeholders in the distributed and utility-scale wind industries, the emerging airborne wind energy field, grid integration, power systems modeling, environmental modeling, national laboratories, and academia. The data were produced using the Weather Research and Forecasting (WRF) Model. The vertical grid used in WTK-LED includes many vertical layers in the atmospheric boundary layer to provide information on atmospheric quantities across the rotor layer of utility-scale and distributed wind turbines. WTK-LED includes:

- **WTK-LED CONUS and WTK-LED Alaska**: Numerical simulations of wind speed and other meteorological variables covering the contiguous United States (CONUS) and Alaska, with high-resolution (5-minute [min], 2-kilometer [km]) data for 3 years (2018–2020) from 10 to 1,000 m above ground level.
- **WTK-LED Climate**: Climate simulations from Argonne National Laboratory covering North America, including Alaska, Canada, and most of Mexico and the Caribbean islands. These simulations complement the new WTK-LED to offer a 4-km, hourly dataset covering 20 years (2001–2020) from 10 to 1,000 m above ground level.
- **NOW-23**: Specific long-term, high-resolution offshore simulations have been conducted separately for the U.S. coasts, Hawaii, and the Great Lakes, leading to the 2023 National Offshore Wind dataset (NOW-23). The data for Hawaii include land-based data and are part of WTK-LED Hawaii. NOW-23 is a 2-km, 5-min dataset from 10 – 500 m above ground level.

Note that the original WIND Toolkit was developed for grid integration studies; it therefore mimicked forecast errors and contained power forecasts alongside meteorological "actuals." The WTK-LED was developed as a meteorological reanalysis-type dataset that satisfies the needs of many stakeholders, such as those in the distributed and utility-scale wind industry, the emerging airborne wind energy field, grid integration, power systems modeling, environmental modeling, and academia. As such, it was not tailored specifically to grid integration studies. Users should be aware of this difference between the WIND Toolkit and WTK-LED and are encouraged to follow the authors' recommendations for use documented in this report (Table ES-1).

Because the accuracy of simulations from a mesoscale model such as WRF varies depending on location and weather situation, and because the model bias or errors can reach up to several meters per second for wind speed, we provide simulated wind speed uncertainty estimates to use in conjunction with the deterministic model simulations. Sixteen ensembles were run over CONUS, Alaska, Hawaii, and other areas in North America to estimate both the model structural uncertainty and uncertainty due to internal model variability. Structural uncertainty results from unknowns in the physics parameterizations used in the model. Internal variability results from the nonlinearity in the equations that underpin the weather forecasting models. Thus, when using different physics parameterizations or different initial conditions, models can generate different

solutions. The estimates of the simulated wind speed uncertainty can be valuable for assessing distributions of simulated wind speeds per model grid point.

In summary, we found that summer generally exhibits lower wind speeds than other seasons, while winter shows higher wind speeds than other seasons. However, summer has higher model internal variability, whereas winter has lower model internal variability but larger structural uncertainty. We also found that the larger model domain (i.e., North America Climate domain) shows larger internal variabilities and structural uncertainties (especially in the summer) than the smaller model domain (i.e., CONUS or Alaska). Comparing the two sources of uncertainty over the same domain and same season, the physics uncertainty is larger than the uncertainty from model internal variability in general but depends on specific locations. The uncertainty range due to internal variability does not change significantly when using different physics schemes, when using different forcing data, or in a different year. In general, the model uncertainty is much larger for shorter timescales, such as days or hours, and is smaller on a weekly, monthly, or seasonal scale.

The WTK-LED is available in NREL's Wind Resource Database, an interactive web platform, at https://wrdb.nrel.gov/. Additionally, the WTK-LED data are available on OpenEI (https://data.openei.org/submissions/2) and can be accessed via an AWS Public Dataset Bucket. The Wind Resource Database also houses the original WIND Toolkit, which provides time series of meteorological variables every 5 min and every 2 km across CONUS from 2007 to 2013.

This report focuses on a description of (1) the land-based WTK-LED for CONUS, Hawaii, and Alaska at a spatial resolution of 2 km and a temporal resolution of 5 min, (2) the 20-year WTK-LED Climate dataset covering North America at a spatial resolution of 4 km and temporal resolution of 1 hour, and (3) the methods of uncertainty quantification and expression. We also provide limited model validation results, as we are preparing a rigorous validation to be published in an upcoming journal article. **Data users are strongly advised to perform a priori validation of the data based on their needs**. Following our validation results to date, we suggest use cases and applications for each dataset of the WTK-LED as shown in Figure ES-1:

Table ES-1. Suggested Use Cases for the High-Resolution 3-Year WTK-LED Datasets, the Hourly 4-km WTK-LED Climate Dataset, and the NOW-23 Offshore Dataset. A priori validation of the data is strongly recommended.

Dataset	WTK-LED CONUS and WTK-LED Alaska	WTK-LED Climate	NOW-23
Description	Simulations from 2018 to 2020 at 5 min and 2 km resolution	Simulations covering North America from 2001 to 2020 at hourly and 4 km resolution	Simulations at 5 min and 2 km resolution for offshore areas and Hawaii for 20+ years
Use case: wind resource assessments	Preliminary land-based wind resource assessments including interannual, seasonal, diurnal variability assessments	Averaged wind resource estimates (e.g., interannual variability, long-term averaged seasonal and diurnal variabilities); Applications needing high-resolution data covering North America	Preliminary offshore wind resource assessments, including interannual, seasonal, diurnal variability assessments
Use case: grid integration	Land-based grid integration studies	Avoid time-specific grid integration analyses	Offshore grid integration studies
Use case: environmental modeling and airborne wind energy	Environmental modeling (the data include vertical wind speed and turbulence kinetic energy) or airborne wind energy assessments (the data are available up to 1000 m above ground level)	Vertical wind speed and turbulence kinetic energy is not available.	Offshore studies requiring data up to 500 m; vertical wind speed and turbulence kinetic energy not included
Use case: statistical weather analyses	Shorter-term (up to 3-year) statistical analyses	Risk analysis about wind extremes due to natural hazards (hurricanes, wildfire)	Risk analysis about wind extremes due to natural hazards (hurricanes)

Table of Contents

List of Figures

List of Tables

1 Introduction

Wind energy has experienced extensive growth over the last decades, and as more wind farms are built over land and offshore, existing gaps in wind energy research will need to be addressed in the years to come (Veers et al. 2022). Various stakeholders in the wind energy community rely on atmospheric datasets, such as those in the distributed and utility-scale wind industry, the emerging airborne wind energy field, grid integration, power systems modeling, environmental modeling, and academia. They use these datasets to analyze weather conditions and wind resources in their regions of interest—from seasonal trends down to the 5-minute (min) variability of wind speeds. In the absence of measurements that would describe atmospheric conditions over large areas, the atmospheric datasets are simulated, mostly with numerical weather prediction models.

In an attempt to create a dataset that fits many needs, in particular the needs of the stakeholders in grid integration, the original Wind Integration National Dataset (WIND) Toolkit (Draxl et al. 2015a) was designed as the most up-to-date and largest freely available grid integration dataset at the time of its creation. It provides time series of meteorological variables every 5 min and every 2 kilometers (km) across the contiguous United States (CONUS) in the 7 years spanning 2007 to 2013. It also includes power forecasts for selected sites. The WIND Toolkit was created with the Weather Research and Forecasting (WRF) Model (Skamarock and Klemp 2008, https://www.mmm.ucar.edu/models/wrf), simulating CONUS in one model domain to avoid spatial seams. The computational expense was huge, and at the time, the WRF code was modified to use parallel asynchronous input/output to keep pace with the continuous generation of output data resulting from very high spatial and temporal resolutions.

Since its release, the WIND Toolkit has been widely used across academia, industry, and national laboratories for various applications. The two primary uses have been wind resource assessment and grid integration studies. For wind resource assessment, the toolkit has been employed to evaluate the feasibility of wind and solar energy integration (McCullough et al. 2024), assess the impacts of siting considerations on offshore wind potential (Zuckerman et al. 2023), estimate offshore wind speeds (James, Benjamin, and Marquis 2018), compare different wind resource assessment methods (Pronk et al. 2022), and investigate the potential for wind and solar to replace coal (Morse et al. 2022). Researchers have also used it to examine the influence of land use and turbine technology on wind potential (Lopez et al. 2021), quantify uncertainty in wind resource modeling (Bodini, Castagneri, and Optis 2023), characterize offshore wind power potential (Wang et al. 2022), detect and characterize sea breezes (Xia et al. 2022), and assess the resource and load compatibility of wind energy (Ortega et al. 2020). In grid integration analyses, the WIND Toolkit has been used to assess wind resources at specific locations and how they might complement existing grids (Douville and Bhatnagar 2021; Novacheck and Schwarz 2021; Mai et al. 2021) and to explore the economic and technical challenges of integrating offshore wind into existing grid infrastructure (Beiter et al. 2020a, 2020b). Additionally, studies have used the toolkit to investigate wind power variability (Yuan 2020; Boretti and Castelletto 2020) and the impact of forecasting accuracy on grid stability (Wang et al. 2016). For modeling and optimization, researchers have used the toolkit to optimize grid planning and operation with wind energy (Maloney et al. 2019; Satkauskas et al. 2022).

The WIND Toolkit has also contributed significantly to wind power forecasting research: it has been used to develop and evaluate short-term forecasting algorithms (Perr-Sauer et al. 2020), create probabilistic forecasts (Sun, Feng, and Zhang 2020), characterize wind site forecast-ability (Feng et al. 2019), and analyze the diversity of wind time series data (Feng et al. 2017). The toolkit has further been applied to distributed wind energy research, with studies investigating short-term forecasting for distributed wind (Sheridan et al. 2024), exploring challenges in resource assessment for distributed wind turbines (Phillips et al. 2024), and validating wind resource and energy production simulations (Sheridan et al. 2022). Other applications include research tailored to wind power plants, where it has been used to optimize layouts (Stanley et al. 2022), understand impacts (Abraham and Hong 2021), model performance (Hawbecker, Basu, and Manuel 2017), and evaluate economics (Hamilton et al. 2020). The WIND Toolkit has also supported airborne wind energy research (e.g., Weber et al. 2021), and artificial intelligence/machine learning applications for wind resource assessment (Frech et al. 2024), high-resolution data creation (Benton et al. 2024), and optimization of wind plant layouts (Harrison-Atlas et al. 2024). Lastly, the WIND Toolkit has been used to study legal and environmental aspects of wind energy, including laws, siting challenges (Stahl and Chavarria 2009; Andriano 2009), and environmental impacts like bat detection strategies (Rabie et al. 2022). It has also been employed in evaluating the value of hybrid energy systems, such as those combining wind energy with solar and storage (Schleifer et al. 2023; Riccobono 2023).

The meteorological WIND Toolkit is a deterministic dataset, i.e., it provides one value for each atmospheric variable at each time stamp per 2-km grid cell. In the absence of widely available measurements, especially at hub height, the modeling error is mostly unknown, except for sites where validation studies have been carried out (e.g., Draxl et al. 2015b).

Over the years, various other public datasets have been used by stakeholders, such as reanalysis datasets (e.g., the European Centre for Medium-Range Weather Forecasts Reanalysis v5 [ERA5; Hersbach et al. 2020], ERA-Interim, Modern-Era Retrospective analysis for Research and Applications [MERRA; Millstein et al. 2023]), or the High-Resolution Rapid Refresh (HRRR) model output developed by the National Oceanic and Atmospheric Administration (n.d.). Recently, CONUS404, a 4-km reanalysis dataset over the conterminous United States was produced by the National Center for Atmospheric Research (Rasmussen et al. 2023). A report published by the Energy Systems Integration Group (2023) compared many of these widely used datasets for power system applications. They showed that all the datasets have some of the required characteristics needed for wind energy applications, and that all also have shortcomings. For example, the HRRR seems to have the appropriate resolution, but because it is an operational forecasting product, the many code updates and improvements make its performance and bias change over the years. None of the products mentioned above include uncertainty information, and none but the WIND Toolkit are available at a temporal resolution of less than 1 h.

To satisfy a wide range of stakeholders across various wind energy disciplines and to close some of the gaps that current public datasets have, we aimed to develop an updated version of the meteorological WIND Toolkit. The updated WIND Toolkit, named WIND Toolkit Long-term Ensemble Dataset (WTK-LED), is a collection of meteorological datasets with specific spatial and temporal resolutions. WTK-LED includes model uncertainty and interannual wind speed variability at every modeling grid point to give users a range of possible wind speeds. WTK-LED includes:

- Numerical simulations of wind speed and other meteorological variables covering CONUS and Alaska with high-resolution (5-min, 2-km) data available for 3 years (2018–2020): WTK-LED CONUS, WTK-LED Alaska. Note that some non-wind-related meteorological variables are made available hourly only (see Section 5.3).
- Climate simulations covering the North American continent, including Alaska, Canada, and most of Mexico, and the Caribbean islands. These simulations complement the new WTK-LED to offer a 4-km, hourly dataset covering 20 years, from 2001 to 2020: WTK-LED Climate.
- Specific long-term, high-resolution offshore simulations have been conducted separately for the U.S. coasts, Hawaii, and the Great Lakes, leading to the 2023 National Offshore Wind dataset: NOW-23. The data for Hawaii include land-based data and are part of WTK-LED Hawaii.

Note that the original WIND Toolkit was developed for grid integration studies; it therefore mimicked forecast errors and contained power forecasts alongside meteorological "actuals." The WTK-LED was developed as a meteorological reanalysis-type dataset that satisfies the needs of many stakeholders. As such, it was not tailored to grid integration studies. Users should be aware of this difference between the WIND Toolkit and WTK-LED and are encouraged to follow the authors' recommendations for use documented in Section 6 Discussion. Table 1 summarizes the differences between WTK-LED and the WIND Toolkit, which has been widely used to date. More details can be found in Section 6 Discussion. The reader is referred to Cox et al. (2018) for information on the limitations and benefits of various types of data in renewable energy analyses to support informed renewable energy decision-making.

Table 1. Characteristics of WTK-LED vs. WIND Toolkit

	WTK-LED CONUS, Alaska, Hawaii	WTK-LED Climate	WIND Toolkit
WRF version	4.1.3 and 4.2.1	4.2.1 for the 20-years, 4.1.3 for the ensemble	3.4.1
Simulated period	2018–2020	2000–2020	2007–2013
Boundary conditions for WRF simulations	ERA5, no nudging	ERA5, no nudging	ERA Interim, spectral nudging
Model uncertainty	Ensemble run over Alaska and Hawaii	Ensemble	Deterministic dataset
Region covered	CONUS, Alaska, Hawaii	North America	CONUS
Dataset	Meteorological	Meteorological	Meteorological and power forecasts
Suggested use	Preliminary wind resource assessments (a priori validation of data strongly recommended), risk analysis about wind extremes due to natural hazards (e.g., hurricanes); can be used for grid integration studies	Risk analysis about wind extremes due to natural hazards; wind resource estimates (interannual variability, long-term averaged seasonal and diurnal variabilities); applications using high-resolution data covering a big geographical area; avoid weather-scale applications or time-specific grid integration analyses	Developed as a grid integration dataset to mimic forecast errors; meteorological dataset has been used for resource assessments (a priori validation of data strongly recommended)

The creation of WTK-LED was initially funded by the Distributed Wind Tools Assessing Performance project (NREL n.d.). The initial intent was to provide a resource dataset to the distributed wind community, focusing on modeling winds for hub heights lower than 100 meters (m). Stakeholders across other disciplines, such as utility-scale wind and airborne wind energy, grid integration, power systems modeling, and environmental modeling, also expressed the need for an updated WIND Toolkit. The vertical grid used in WTK-LED therefore includes more vertical layers than are available from commonly used reanalysis products, which is important to accurately model winds across the rotor layer of utility-scale and distributed wind turbines. The final dataset is available for heights up to 1,000 m. Funding for the NOW-23 dataset came from the National Offshore Wind Research and Development Consortium and the Bureau of Ocean Energy Management. Funding for the computation of the 4-km dataset came from the Argonne Leadership Computing Facility, and dataset analysis was supported by the Argonne Climate Action Initiative and the Tools Assessing Performance Project.

Because the NOW-23 dataset is documented separately (Bodini, Castagneri, and Optis 2023; Bodini et al. 2022; Bodini et al. 2024), this report focuses on a description of the land-based WTK-LED for CONUS and Alaska for the 3-year, 2-km/5-min dataset, the NOW-23 2-km/5-min Hawaii simulations, and the WTK-LED Climate 20-year 4-km/hourly dataset. Section 2 describes the methods used to create the data, including the ensemble runs. Data validation results are presented in Section 3, followed by a detailed description of our uncertainty quantification in Section 4. NREL developed a novel web platform to make the data publicly available, which is highlighted in Section 5. The discussion in Section 6 provides users with guidance on which datasets to use for their specific needs. Section 7 includes summary and conclusions.

2 Data and Methods

The WTK-LED was simulated using the WRF model. WRF modeling necessitates assumptions and tradeoffs with regards to model setup, resolution, and computation. The steps of dataset creation are portrayed in Figure 1. First, to establish the best balance of assumptions and tradeoffs, we convened a WRF expert steering committee comprising modeling experts from Pacific Northwest National Laboratory, Argonne National Laboratory (Argonne), National Renewable Energy Laboratory (NREL), and the University of Colorado Boulder to discuss the WRF settings to consider. To identify the most important model setups and physics in the WRF model with implications for wind energy, we conducted 10 tests over a relatively small domain using various physics parameterizations (land surface models and planetary boundary layer schemes) and boundary conditions (i.e., ERA5, MERRA2). We conducted the tests for June 2018 over the southern Great Plains using different spatial resolutions (2 and 4 km), with and without spectral nudging. June 2018 was chosen because of the frequently observed low-level jets passing through the selected region. We then evaluated the tests using observations and calculated bias, root-mean-square error (RMSE), mean absolute error (MAE), and correlation, and identified a setup using the Noah land surface model (LSM) and the Yonsei University (YSU) planetary boundary layer (PBL) scheme. We selected an additional setup with the Mellor-Yamada-Nakanishi-Niino (MYNN) PBL scheme (which was important for the output of turbulence kinetic energy [TKE] and because it has been improved over the last few years for wind energy applications [Olsen et al. 2019]). Out of those 10 experiments, 6 were selected that cover the best- and worst-performing setups and the middle of all members with the goal of covering a range of uncertainties by considering the overall performance. We also performed an analysis of wind speed differences between the long-term means of HRRR, Vortex data from the Global Atlas of the International Renewable Energy Agency (n.d.), and the original WIND Toolkit to determine trends and whether the simulations performed reasonably. Finally, the best setup was used to create simulations from 2018 to 2020, which were reinitialized monthly. On an ongoing basis we compared the simulations with observations at selected grid points, and we compared averages to Vortex data and the original WIND Toolkit to make sure the simulations were behaving as expected.

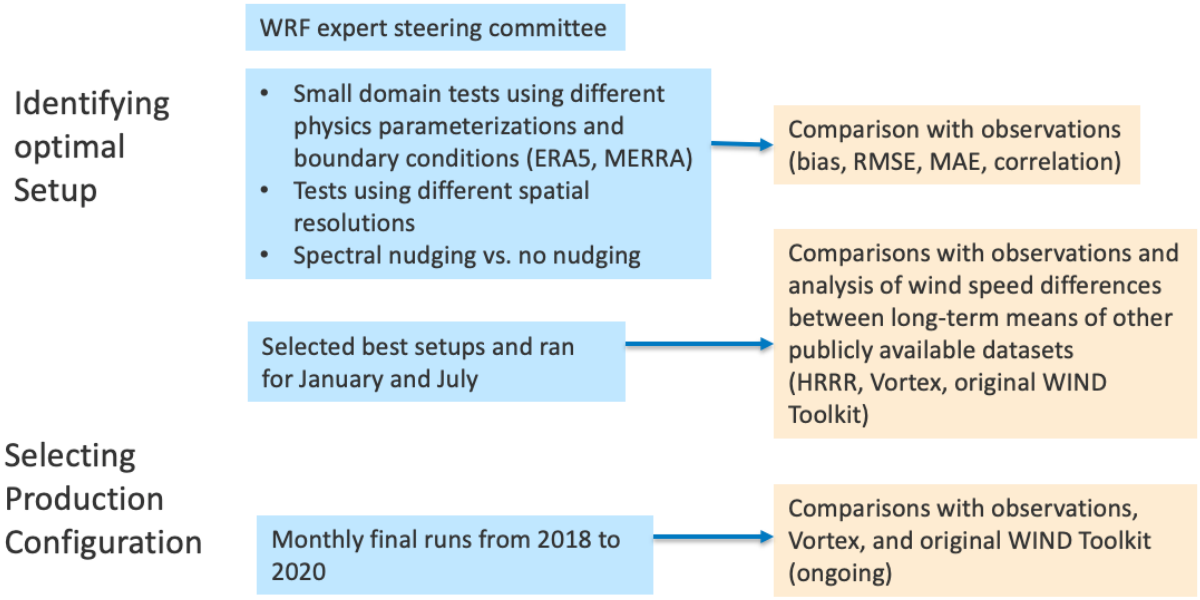

Figure 1. Creation of the land-based WTK-LED

2.1 WRF Setup

The WRF model versions 4.1.3 and 4.2.1 were used to perform the numerical simulations. The model performance between these two versions is very similar. A single domain was forced by ERA-5 (Hersbach et al. 2020) boundary conditions for the CONUS, Alaska, and North America simulations every 3 h. Two nested domains were used over Hawaii to match the NOW-23 Hawaii simulation setup (Bodini et al. 2024). For all but the North America climate simulations, the model was run with 61 vertical levels; the levels relevant for heights where most wind turbines operate are at approximately 6 m, 23 m, 42 m, 59 m, 75 m, 94 m, 117 m, 145 m, 176 m, 212 m, 252 m, and 297 m. North America climate simulations have 49 vertical levels; those relevant for hub heights are at approximately 8 m, 24 m, 40 m, 57 m, 73 m, 101 m, 141 m, 182 m, 223 m, and 265 m. The final files made available to the public were postprocessed and contain variables interpolated to specific heights (Section 5.3).

We tested several options for running the WRF model, including (1) spectral nudging, (2) the frequency of the boundary conditions (3 h versus 6 h), (3) the need for 2-km resolution simulations compared to 4-km and coarser spatial resolutions, (4) the frequency at which the data should be stored to capture the short-term variations in the wind fields and obtain estimates of computing resources needed, and (5) different data sources for boundary conditions. For the creation of the original WIND Toolkit (Draxl et al. 2015a), nudging was considered crucial to avoid model drift in long-term simulations (e.g., months, decades). However, nudging is computationally very expensive and can add 25%–40% of the computational cost, depending on the size of the model domain. An alternative way to maintain the model performance and keep the cost reasonable is to reinitialize the model and let it run for a relatively short time with a sufficient spin-up time (Pan et al. 1999; Qian, Seth, and Zebiak 2003; Lo, Yang, and Pielke 2008). The number of rows for specified boundary value nudging was set to 10 to account for the fact that we used only one modeling domain. The WTK-LED CONUS, Alaska, and Hawaii

simulations were reinitialized every month, with 2 days of spin-up time and simulation times of 1 month to create overlap to average over the seams that are created by restarting the model. Such seams could lead to artificial ramps in simulations of wind speed and other variables, especially at model outputs every 5 min. Tests showed no model drift within the 1-month periods; hence, nudging was not selected for the final runs. The 20-year-long WTK-LED Climate simulations were reinitialized every year and run for 14 months continuously without nudging, and with the first 2 months from previous years (November and December) as spin-up time. The reason for this decision was mainly due to the large demand of computational expense. We updated the boundary conditions more frequently (every 3 h) than typically done (e.g., every 6 h). We saved the data every 5 min for the final production runs from 2018 to 2020. For the ensembles that were used to estimate model uncertainty, we output data every 15 min.

The WRF physics settings for the WTK-LED CONUS and Alaska simulations include the Morrison double-moment scheme, the Rapid Radiative Transfer Model (RRTMG) longwave and shortwave radiation schemes, the MYNN level 2.5 PBL and surface layer schemes, and the Unified Noah LSM. The cumulus parameterization was turned off because the spatial resolution is sufficient to explicitly resolve the convections. No upper damping was selected. A time-varying sea surface temperature was chosen. We used a 3*dx exponential decay factor for the relaxation zone ramp. The radiation time step was set to 15 s. WTK-LED Hawaii uses a similar setup except that it uses 2 nested domains and Ferrier microphysics as well as the Kain-Fritsch cumulus parameterization for the outermost domain. The WTK-LED Climate simulations use a setup similar to the WTK-LED CONUS simulations, covering a significantly larger area comprising the North American continent and surrounding oceans, including Alaska, Canada, most of Mexico, and the Caribbean Islands. They use the YSU PBL scheme with topographic correction for surface winds to represent extra drag from subgrid topography and enhanced flow at hilltops, and the revised MM5 surface layer scheme. The spatial and temporal resolutions are not as high as for WTK-LED CONUS, given it was developed for studying climate variability and climate change (see more details in Akinsanola et al. 2024). Table 2 lists the differences between the WTK-LED simulations.

Table 2. WRF Setup of the CONUS, Alaska, Hawaii, and North America Climate Simulations

Name list details can be found in the Appendix.

	CONUS	Alaska	Hawaii	North America
Available period	2018–2020	2018–2020	2000–2019	2001–2020
WRF version	4.1.3	4.1.3	4.2.1	4.2.1
Restarts	48 h before the start of the month	48 h before the start of the month	48 h before the start of the month	yearly every November 1
Temporal resolution	5 min	5 min	5 min	1 h
Spatial resolution	2 km	2 km	6 km to 2 km	4 km
Nested domains	1	1	2	1
Vertical levels	61	61	61	49
PBL scheme	MYNN level 2.5	MYNN level 2.5	MYNN level 2.5	YSU + topographic correction for wind speed
Cumulus parameterization	-	-	Kain-Fritsch only in domain 1	-
Microphysics scheme	Morrison	Morrison	Ferrier	Morrison

We found that using MERRA-2 boundary conditions did not improve the simulations when compared with observations, and due to the computational expense of the simulations, the team opted not to conduct simulations with boundary conditions other than ERA5.

2.1.1 WTK-LED CONUS: High-Resolution Simulations Covering CONUS at 2-km/5-min Resolution

The simulation domain covering CONUS consists of 2,650 × 1,950 grid points (Figure 2) and covers the years 2018–2020. The WRF setup was the one explained in Section 2.1, using the specific parameters from Ensemble 1 (Table 2).

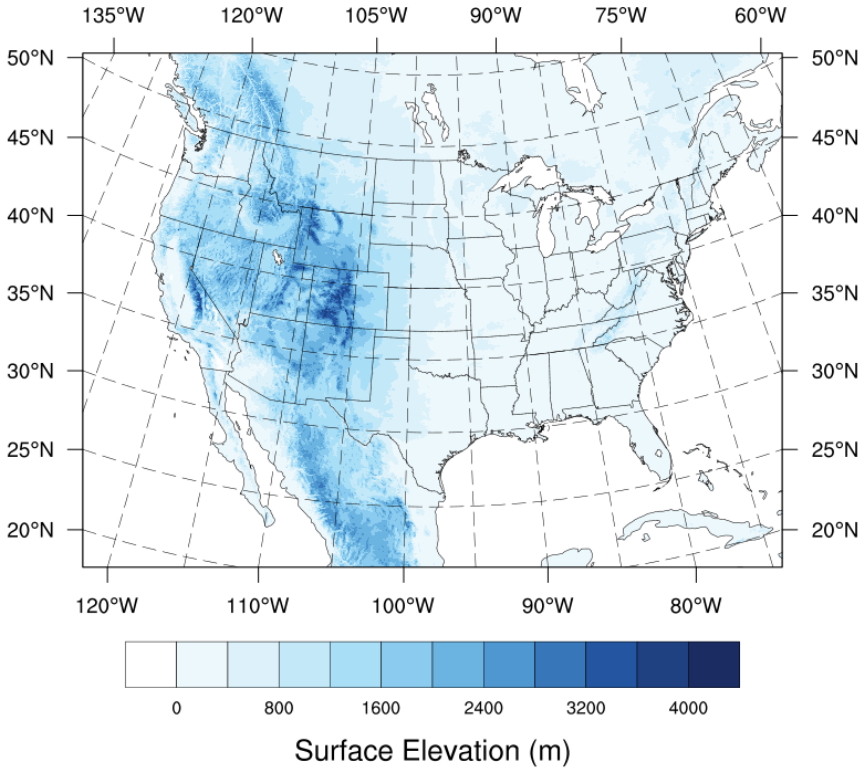

Figure 2. WRF model domain for CONUS at a spatial resolution of 2 km, with 2,650 × 1,950 grid points along the west-east and south-north directions

2.1.2 WTK-LED Alaska: High-Resolution Simulations Covering Alaska at 2-km/5-min Resolution

The simulation domain covering Alaska consists of 1,889 × 1,419 grid points (Figure 3). The WRF setup was the one explained in Section 2.1, using the specific parameters from Ensemble 1 (Table 2). The simulations were run for 2018–2020.

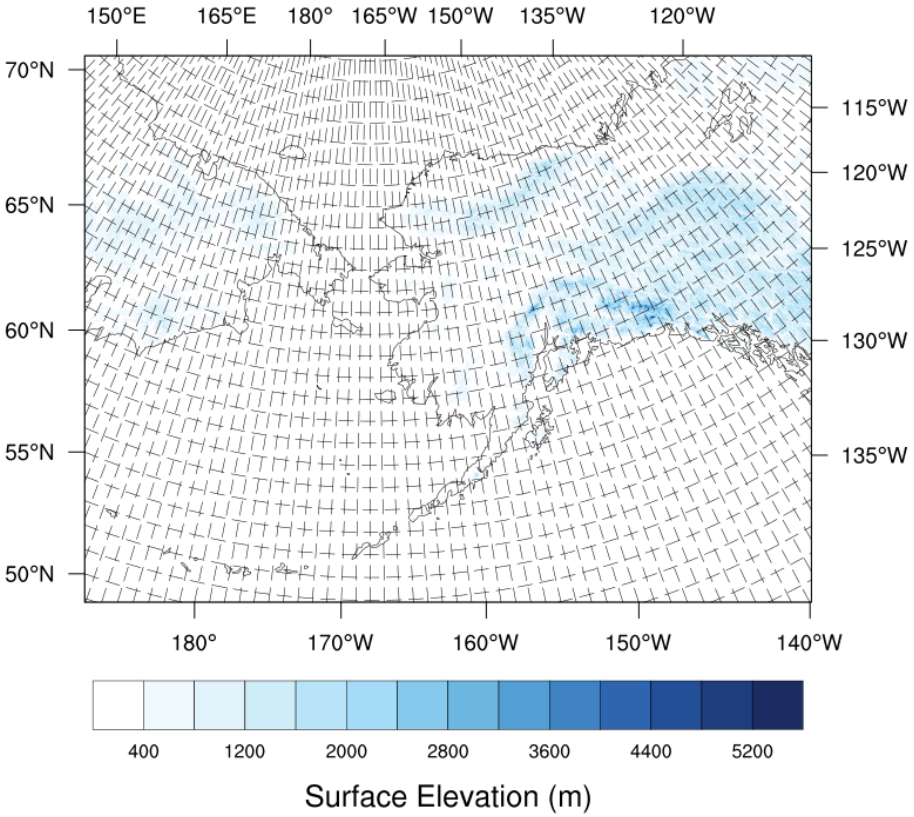

Figure 3. WRF model domain for Alaska at a spatial resolution of 2 km, with 1,889 × 1,419 grid points along the west-east and south-north directions

2.1.3 WTK-LED Hawaii: Long-Term, High-Resolution Simulations Covering Hawaii at 2-km/5-min Resolution

The 20-year (2000–2019) Hawaii simulations were conducted for and funded by the National Offshore Wind Research and Development Consortium project and are now part of the NOW-23 dataset (Bodini et al. 2023). These simulations and their model setup were conducted and decided upon prior to the development of the WTK-LED. Consequently, the model setup is slightly different from what is used in the rest of the WTK-LED dataset. The simulation domain covering Hawaii consists of 309 × 283 grid points in Domain 1 with grid spacing of 6 km, and 727 × 649 grid points in Domain 2 with grid spacing of 2 km (Figure 4). Differences to the model setup compared to the CONUS simulations include the use of WRF version 4.2.1, the Ostia sea surface temperature product, the Ferrier microphysics scheme, and the Kain-Fritsch cumulus parameterization in Domain 1. More details about the NOW-23 simulation setup can be found in Bodini et al. 2024.

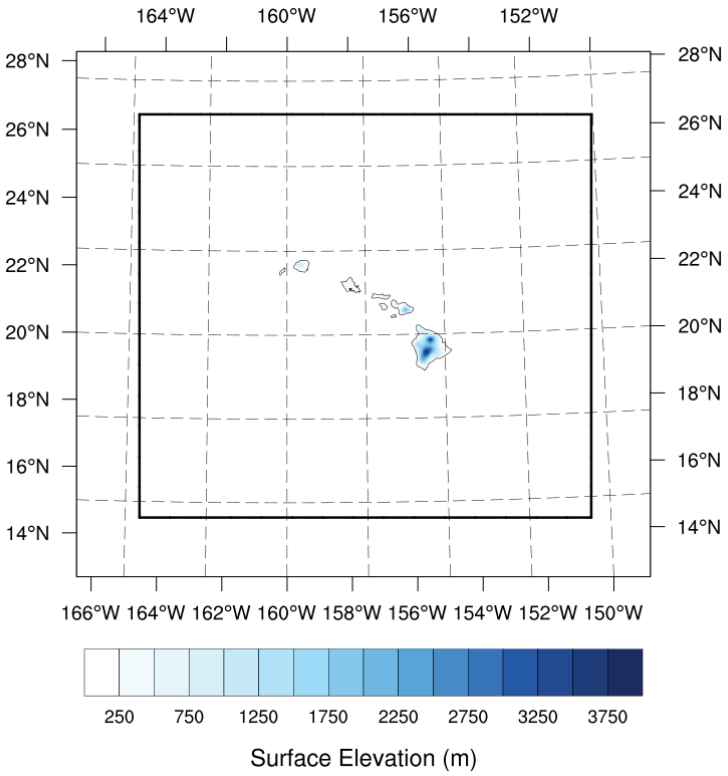

Figure 4. Hawaii model domain. The outer domain has 6-km grid spacing, and the inner domain has 2-km grid spacing.

2.1.4 WTK-LED Climate: Long-Term, High-Resolution Simulations Covering North America at 4-km/Hourly Resolution

Simulations were conducted covering the North American continent and surrounding oceans, including Alaska, Canada, most of Mexico, and the Caribbean islands. These simulations were conducted by Argonne and constitute first-time climate-scale simulations using ultrahigh spatial resolutions (4 km per grid cell, convection-resolved scale). The simulation domain spans 2,050 × 1,750 grid points (Figure 5). These calculations will directly support the National Climate Assessment 5 process that is currently underway because they can explain the physical mechanisms driving the precipitation intensity increase observed in the continental United States for improved climate assessments. The data are built on a previous climate dataset, called Argonne Downscaled Data Archive, supported by the U.S. Department of Defense Strategic Environment Research and Development Program, at 12 km, considering a series of model uncertainties. The data have supported multiple federal and industry projects and have been extensively evaluated (e.g., Zobel et al. 2018; Wang and Kotamarthi 2015; Wu et al. 2022; Pringle et al. 2021). The recently completed 4-km data are found to show better performance with smaller bias for wind, precipitation, hurricane intensity and eyewall features (Akinsanola et al. 2024; Tobias-Tarsh et al. 2023; Jung et al. 2023). The 4-km data also support the PR100 project (Puerto Rico Grid Resilience and Transition to 100% Renewable Energy), which aims to develop 100% renewable energy in Puerto Rico considering climate change risks. These simulations serve as the long-term dataset for the WTK-LED.

The North America simulations use the same initial and boundary conditions as the 2-km/5-min run over CONUS. They also employ similar physics parameterizations and model setup as described in Section 2.1, except that they have 49 vertical levels (the lowest levels relevant for wind energy applications are at 7 m, 22 m, 37 m, 52 m, 67 m, 93 m, 131 m, 169 m, 207 m, 245 m, 284 m, and 322 m). They use the YSU PBL scheme with topographic correction for surface winds to represent extra drag from subgrid topography and enhanced flow at hilltops, and the revised MM5 surface layer scheme.

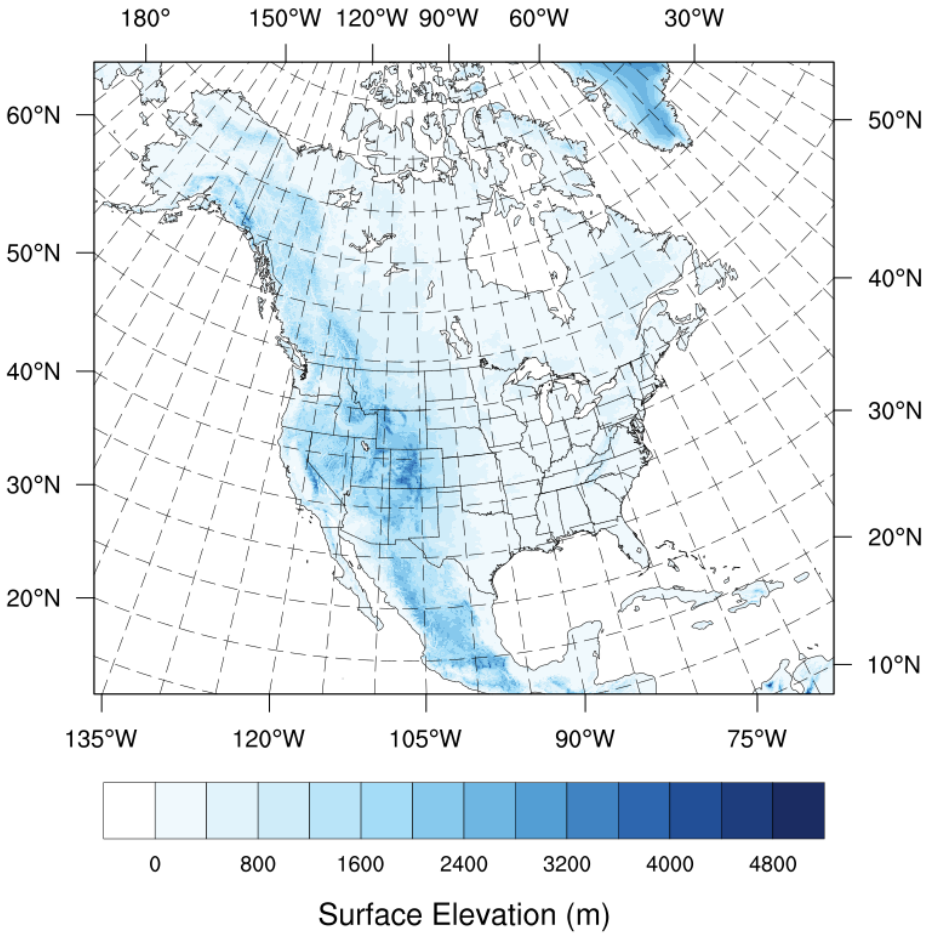

Figure 5. Model domain for North America at a grid spacing of 4 km, with 2,050 × 1,750 grid points along the west-east and south-north directions

2.2 Ensemble Runs for Uncertainty Quantification

Depending on the region, topography, and weather situation, even if optimized for a region, mesoscale WRF model output can only be expected to be accurate (e.g., RMSE) within 0.5 m/s to about 2 m/s. Therefore, the team was motivated to provide model uncertainty estimates to the community to be used in conjunction with the deterministic model simulations.

Ensembles were set up over CONUS, Alaska, Hawaii, and North America to estimate both the model structural uncertainty and uncertainty due to model internal variability. Structural uncertainty results from unknowns in the physics parameterizations used in the model; internal

variability results from the nonlinearity in the equations that underpin the weather forecasting models (Hawkins and Sutton 2011). When the model is initialized on a different day or at a different hour, it can produce different solutions.

Setting up and running ensembles is one way of quantifying a component of the model uncertainty (compared to the real world) that is linked to the specific WRF setups that were chosen. By using different PBL schemes (YSU and MYNN) as well as various LSM settings that were tested on small domains, we believe that the quantified uncertainty gives the user a decent estimate of the model uncertainty, which can be valuable in assessing the magnitude of possible wind speeds per grid point.

2.2.1 Structural Uncertainty

Structural uncertainty—also referred to as parametric uncertainty in the literature—is due to uncertainty inherent in using a computational model to model the real world. That model contains approximations of the real world to make the science problem tractable and produce solutions in a reasonable amount of time on high-performance computing systems. These approximations, known as parameterizations, are empirical formulations that describe physical phenomena ranging from the movement of air across the planet to the formation of clouds. Multiple options exist in WRF for modeling land surface processes, PBL physics, longwave and shortwave radiation, convection, and cloud microphysics. Regional models require surface layer, PBL, and LSM parameterizations to represent the transfer of heat, moisture, and momentum between the surface and atmosphere (Gilliam and Pleim 2010). The PBL scheme implemented in a model plays a decisive role in the accuracy of forecasted state and flow within the PBL because the wind varies according to the stability and baroclinic instability of the PBL. The surface layer is the lowest part of the atmosphere, typically about a tenth of the height of the PBL, where surface fluxes of scalars and momentum, nearly constant with height in this layer, dominate dynamics and physics. Vertical profiles of scalars and wind are determined by the Monin-Obukhov similarity theory. LSM schemes combine atmospheric information from the surface layer scheme with land surface properties (dependent on land uses) to evaluate the vertical transport done in the PBL schemes, which has a direct influence on the estimation of the PBL height (Han, Ueda, and An 2008). Therefore, we created the ensemble runs by using different combinations of land surface, PBL, and surface layer models. In particular, we used the YSU (Hong and Lim 2006; Noh et al. 2003) and MYNN (Nakanishi and Niino 2006) PBL schemes, which have been used by the authors in past studies and were found to simulate the most realistic local winds and boundary layer characteristics. The Unified Noah LSM (Chen and Dudhia 2001) was selected for land surface processes. It is a four-layer soil temperature and moisture scheme that provides data of sensible and latent heat fluxes in the PBL. In addition, the Noah Multiparameterization (NoahMP) land surface model (Smirnova, Brown, and Benjamin 1997) was used with two options for the dynamic vegetation and surface options.

Based on our analysis, we chose to explore the following physics options for structural uncertainty estimates:

- **PBL schemes:** The YSU PBL scheme (Noh et al. 2003) and the MYNN PBL scheme (Mellor and Yamada 1982; Nakanishi and Niino 2006, 2009) were investigated. YSU is a highly parameterized mixing theory model that does not resolve the turbulence in the model and uses eddy mixing coefficients to represent mixing. This PBL scheme does not

output TKE. The MYNN PBL scheme is a level 2.5 closure scheme for turbulence in the equations and solves for turbulence using parametric equations (not explicitly). It gives estimates of TKE and dissipation rates within the boundary layer of the atmosphere. While mean wind forecasts between these two models would not be expected to deviate significantly, the higher computational costs of MYNN were considered to be necessary to obtain TKE information for wind applications.

- **Land surface models:** The Noah (Chen and Dudhia 2001) and NoahMP (Niu et al. 2011) models were evaluated. Noah relies on both soil and vegetation processes for water budgets and surface energy closures. The model is capable of modeling soil and land surface temperature, snow water equivalent, and the general water and energy fluxes. Noah-MP is an improved version of the Noah LSM and provides better representations of terrestrial biophysical and hydrological processes. Major physical mechanism improvements include improved treatment of soil moisture. Noah-MP is unique compared with the other LSMs, as it can generate hundreds of parameterization schemes through different combinations of processes, including dynamic leaf, canopy stomatal resistance, runoff and groundwater, a soil moisture factor controlling stomatal resistance, and six other processes.

As mentioned in Section 2.1, we initially simulated 10 ensembles over a smaller domain (covering the southern Great Plains), after which we picked ensemble members that generate the highest and lowest wind speeds as well as wind speeds in between all ensemble members. These include six ensemble members, as listed in Table 3, that were the final ensemble members run for the year 2018 to characterize the structural uncertainty.

Table 3. The Six Ensemble Members Run To Determine Structural Uncertainty for 2018

No.	Planetary Boundary Layer Scheme/Land Surface Model	Other WRF Physics Options	Temporal Resolution of Output
1	MYNN2.5/Noah	aer_opt=1 radt=15 swint_opt=1 icloud=1 sst_update=1	5 min
2	YSU/Noah	Same as 1; plus sf_sfclay=1 topowind=1 lsm=1	15 min
3	YSU/NoahMP5-2	Same as 1; plus sf_sfclay=1 dveg=5 opt_sfc=2 topowind=1 lsm=4	15 min
4	YSU/NoahMP5-1	Same as 1; plus sf_sfclay=1 dveg=5 opt_sfc=1 topowind=1 lsm=4	15 min
5	MYNN2.5/NoahMP7-2	Same as 1; plus sf_sfclay=5 dveg=7 opt_sfc=2 lsm=4	15 min
6	MYNN2.5/NoahMP7-1	Same as 1; plus sf_sfclay=5 dveg=7 opt_sfc=1 lsm=4	15 min

2.2.2 Internal Variability

Internal variability comes from the nonlinear physical and dynamical processes that are described by regional scale model equations and develops under given large-scale conditions (Giorgi and Mearns 1991). When there are small changes in model initial conditions, the model solution can be different, especially at short-term forecast scales (e.g., minute-to-hourly and daily scales). This spread in the model output at a given location for a particular time step in the simulation results is referred to as internal variability and is quantified by an ensemble spread represented by ensemble standard deviations (Lucas-Picher et al. 2008; Nikiéma and Laprise 2011; Braun et al. 2012; Wang et al. 2018, Giorgi and Bi 2000).

Wang et al. (2018) have previously studied internal variability in the WRF model by running 16 ensemble members for 3 years. They found clear seasonal cycles in the internal variability, but internal variabilities across years were nearly constant. They also found that the higher the spatial resolution, the larger the internal variability. Similarly, the larger the model domain, the larger the internal variability, because when the model domain is large enough, the regional model will have more freedom to develop its own variability. In contrast, if the domain is small, the model solution would be more constrained by the boundary conditions. In other words, the differences in solutions between two model simulations are higher when the model spatial resolution is higher and the domain size is larger. They also found that a minimum of 10 separate simulations with slightly different initial conditions are required to characterize internal variability. Because the internal variability is spatially dependent, there cannot be a single internal variability measure for the entire modeling domain, especially when the model domain covers multiple climate zones like the United States or North America. Therefore, we have conducted internal variability ensemble simulations for North America to understand the uncertainty due to internal variability over various regions. We have also conducted ensemble simulations for Alaska and Hawaii. These domains are much smaller, so their internal variabilities are expected to be smaller than those generated from the North America domain.

For the WTK-LED, we ran 10 ensemble members with slightly different initial conditions. Specifically, the 10 members start with initial conditions 12 h apart, and the runs were conducted for summer (June to August) and winter (December to February) months, with a spin-up period varying from 3 to 6 days. Table 4 lists the details of the 10 ensembles that were run to determine uncertainty caused by internal variability. ERA5 was used for boundary conditions, and the PBL/LSM schemes and other physics options were the same as for Ensemble 1 from the structural uncertainty simulations (Table 3). The grid spacing was set to 2 km for the CONUS, Alaska, and Hawaii simulations and 4 km for the North America domain, and model output was saved every hour.

Table 4. Ten Ensemble Members of the WTK-LED To Determine Internal Variability in Summer (June to August) and Winter (December to February) Months of 2018

No.	Start of the Simulations for Winter Months	Start of the Simulations for Summer Months
1IV	2017-11-26_00UTC	2018-05-26_00UTC
2IV	2017-11-26_12UTC	2018-05-26_12UTC
3IV	2017-11-27_00UTC	2018-05-27_00UTC
4IV	2017-11-27_12UTC	2018-05-27_12UTC
5IV	2017-11-28_00UTC	2018-05-28_00UTC
6IV	2017-11-28_12UTC	2018-05-28_12UTC
7IV	2017-11-29_00UTC	2018-05-29_00UTC
8IV	2017-11-29_12UTC	2018-05-29_12UTC
9IV	2017-11-29_06UTC	2018-05-29_06UTC
10IV	2017-11-30_00UTC	2018-05-30_00UTC

2.2.3 Ensemble Simulations Covering Alaska

Additional ensemble simulations for Alaska were performed at 2 km for July–December 2018. These simulations will help quantify uncertainty at a higher resolution than the North America ensembles and will therefore help confirm whether the spatial resolution as well as model domain size will impact the uncertainty quantification. To reduce the computational expense, the domain used for these high-resolution ensembles was decreased to cover the majority of Alaska and excluded the very remote Aleutian islands with no living populations (Figure 3).

Additionally, we conducted more tests using the Alaska domain at a grid spacing of 2 km to see whether the internal variability is significantly different if a different physics option is used to run 10 ensemble members: We conducted 10 simulations using the physics setup of Ensemble 3 listed in Table 3. We chose Ensemble 3 because it uses different physics for both PBL and LSM compared to Ensemble 1. Therefore, we had a total of 24 ensemble runs covering structural uncertainties and internal variabilities. The main challenge of producing these ensemble runs was the need for massive computational resources and storage capacities. For example, it takes 1.36 million CPU hours to compute these 24 ensembles for 1 month over the Alaska domain (1,320 × 1,220 × 61 grid cells), generating 2.7 TB of data at 2-km grid spacing and hourly intervals. In Section 4.1, we present the sensitivity of uncertainty estimations to ensemble size using the 24 ensemble runs conducted here.

2.2.4 Ensemble Simulations Covering Hawaii

The domain setup for the Hawaii ensembles matches that for the long-term simulations (Section 2.1). Model output was produced every 15 min for 2018. An ensemble of six members was conducted following Table 3 to capture the majority of the structural uncertainties; a 10-member ensemble was conducted following Table 4 to capture the internal variability. Both ensembles cover the time period of at least summer and winter months.

2.2.5 Ensemble Simulations Covering North America

The 4-km North America model output was characterized for internal variability using 10 internal variability runs for the entire year (January–December). The whole-year simulation approach was used, from Nov. 1 until the end of the next year, because it is anticipated that the internal variability for the Alaska region from the North America setup will be larger than the internal variability using the Alaska domain only. The differences of the ensemble simulations compared to the long-term simulations were the same as listed in Table 3 for structural uncertainty.

3 WTK-LED Validation

Initial validation was carried out for all modeling domains: Alaska, CONUS, North America, and Hawaii. This section summarizes the main validation results. Observations were mostly available at heights lower than typical hub heights for commercial wind turbines (i.e., below 80 m). Limited availability of measurements at hub heights is very typical, as those are often proprietary. The validation results presented here provide a preliminary assessment of the WTK-LED performance, but users are strongly encouraged to perform additional validation studies that are tailored to their applications.

In the validation studies in this section, we focused on the year 2018 because our analysis (not shown) revealed it is a neutral year and can represent general climatology. All three years from 2018 to 2020 are relatively neutral without strong climate oscillations, which is why we simulated these years in WTK-LED CONUS and Alaska. It is crucial to immediately validate model output to detect potential issues in the simulations before many runs were submitted to the high-performance computing system. In addition to comparing WTK-LED model simulations to real-world observations, we also compared them to other publicly available datasets (Table 5). These datasets serve as benchmarks to test whether the WTK-LED follows the overall flow patterns or wind speed distributions. A more comprehensive comparison between these datasets is being prepared for a peer-reviewed journal article by Wang et al. from Argonne.

Table 5. Publicly Available Datasets Used for Comparison With WTK-LED: Their Spatial and Temporal Resolution

Dataset	Spatial Resolution	Temporal Resolution	Remarks
ERA5: https://www.ecmwf.int/en/forecasts/dataset/ecmwf-reanalysis-v5	30 km	hourly	Used as boundary conditions for the WTK-LED WRF simulations; widely used in the wind energy community; global coverage from 1940 to present.
Vortex: https://globalatlas.irena.org/workspace	3 km	monthly averages from 2001 to 2020	Part of the International Renewable Energy Agency Global Wind Atlas; used in the wind energy community; global coverage.
Original WIND Toolkit: https://www.nrel.gov/grid/wind-toolkit.html	2 km	5 min	Produced for grid integration studies, this dataset is considered the dataset the WTK-LED succeeds. The WIND Toolkit is only available from 2007 to 2013 and covers only CONUS.
HRRR: https://rapidrefresh.noaa.gov/hrrr/	3 km	hourly	Operational model simulations, run in forecast mode. Multiple model updates throughout the years, i.e., model performance is not consistent across the years. There are Hawaii, Alaska, and CONUS domains.

3.1 WTK-LED CONUS Validation

We assessed the bias, MAE, and correlation of WTK-LED CONUS at various locations and various heights (Figure 6 and Figure 7) for January 2018. The model output was adjusted to the location and height of the observations via inverse distance weighted interpolation and the power law using temporally varying shear exponents based on the surrounding model heights, respectively. The bias is location-dependent: In certain areas, especially in the complex terrain of NREL's National Wind Technology Center (NWTC) site, the bias is above 2 m/s, whereas certain areas exhibit bias values of less than 0.5 m/s. In general, the simulations exhibit a positive bias, meaning the WTK-LED suggests wind speeds were higher than observed at several observation sites. For most sites, the MAE is higher than that of the ERA5 dataset (differences vary between near zero to ~2 m/s), although for a few sites the opposite is true. Correlation values are, in general, lower than those of ERA5.

Figure 6. Sites used to validate the 5-min, 2-km WTK-LED over CONUS. The height [m] at which the data were validated is indicated for each site.

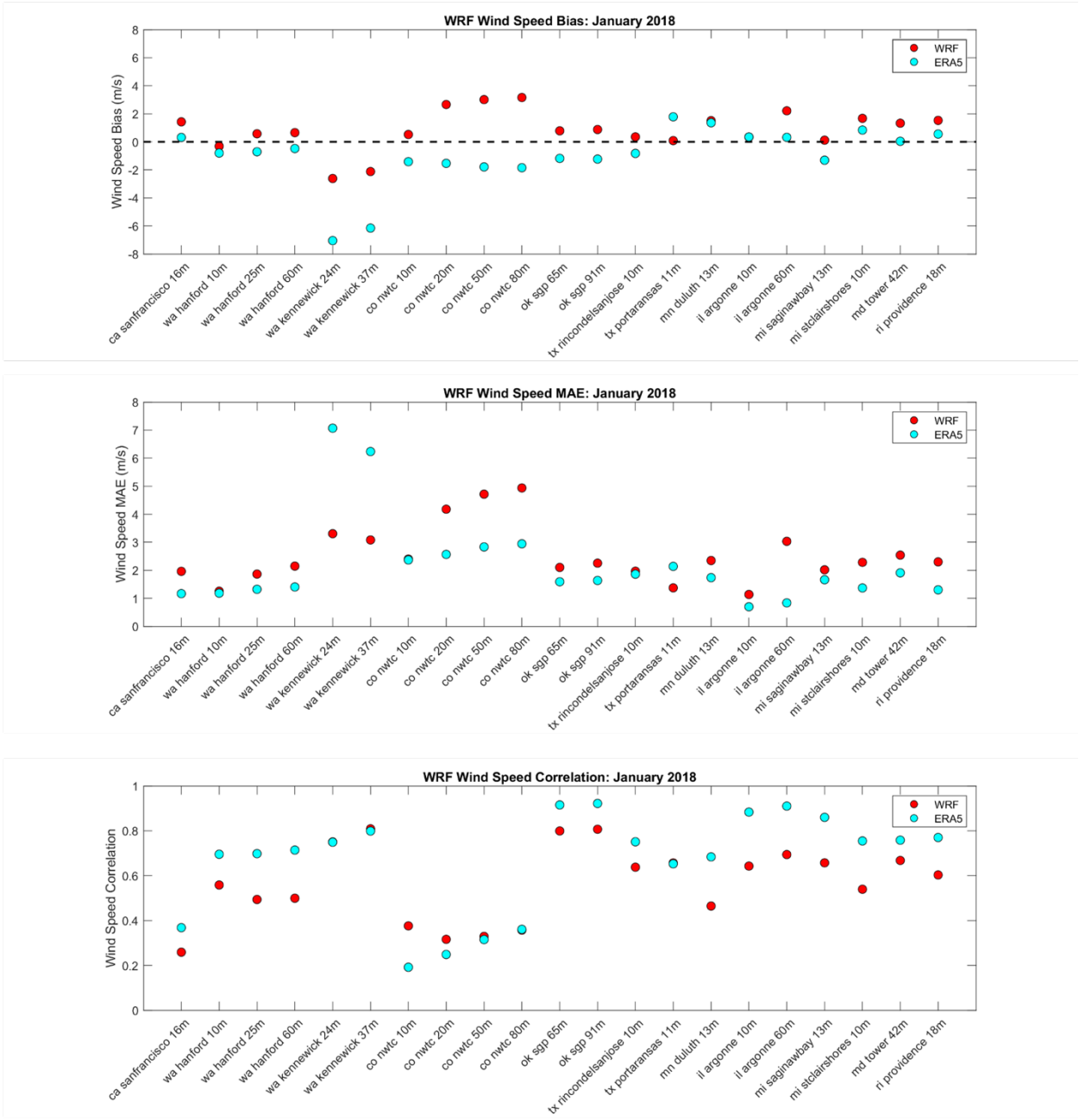

Figure 7. (Top) Wind speed bias (m/s), (Middle) MAE, and (Bottom) correlation for the WTK-LED CONUS ("WRF") (red) and ERA5 data (cyan) at the observation locations used for validation. Data are shown for January 2018.

In addition to comparing WTK-LED model simulations to real-world observations, we also compared them to other publicly available datasets (Table 5). Figure 8 and Figure 9 are examples showing the comparison between WTK-LED CONUS and Global Wind Atlas Vortex. Specifically, we compared 100-m monthly mean wind speed of the WTK-LED CONUS simulation in 2018 with winds at the same height but from long-term (2001–2020) monthly mean Vortex data. Overall, WTK-LED-modeled 100-m winds are slightly higher than the long-term mean in the same month produced by Vortex (ratio larger than 1). This higher wind speed is seen

over the eastern, central, or western United States, depending on the months examined. In general, the geospatial pattern and the magnitude, as well as the seasonality of wind speeds in the Vortex data are well captured by the WTK-LED CONUS simulations.

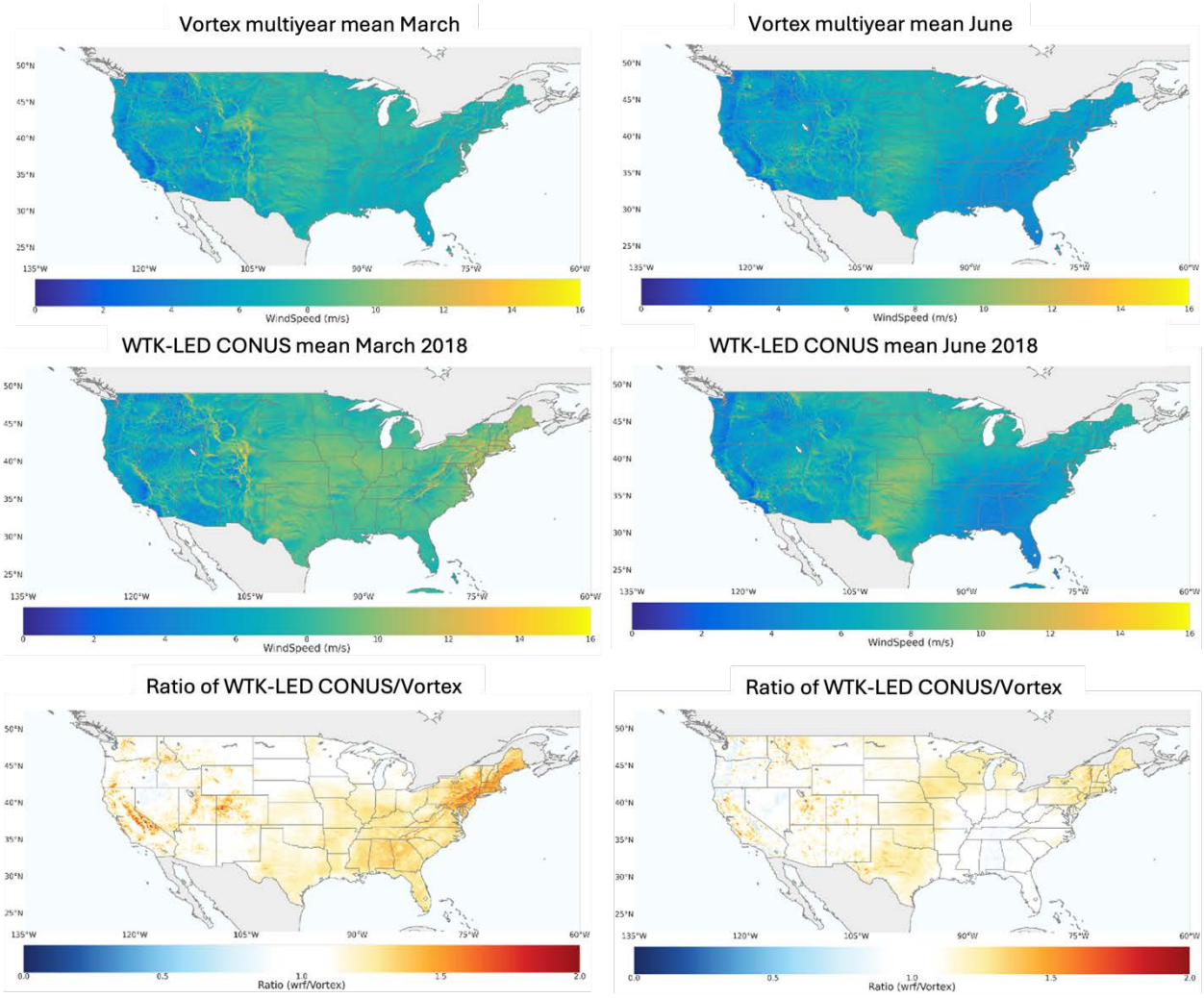

Figure 8. Comparison of 100-m wind speeds between WTK-LED CONUS simulated in 2018 and Vortex long-term mean. The left column maps are for March, and the right column maps are for June. (Top) Vortex multiyear mean. (Middle) WTK-LED CONUS mean for 2018. (Bottom) Ratio of WTK-LED CONUS/Vortex data.

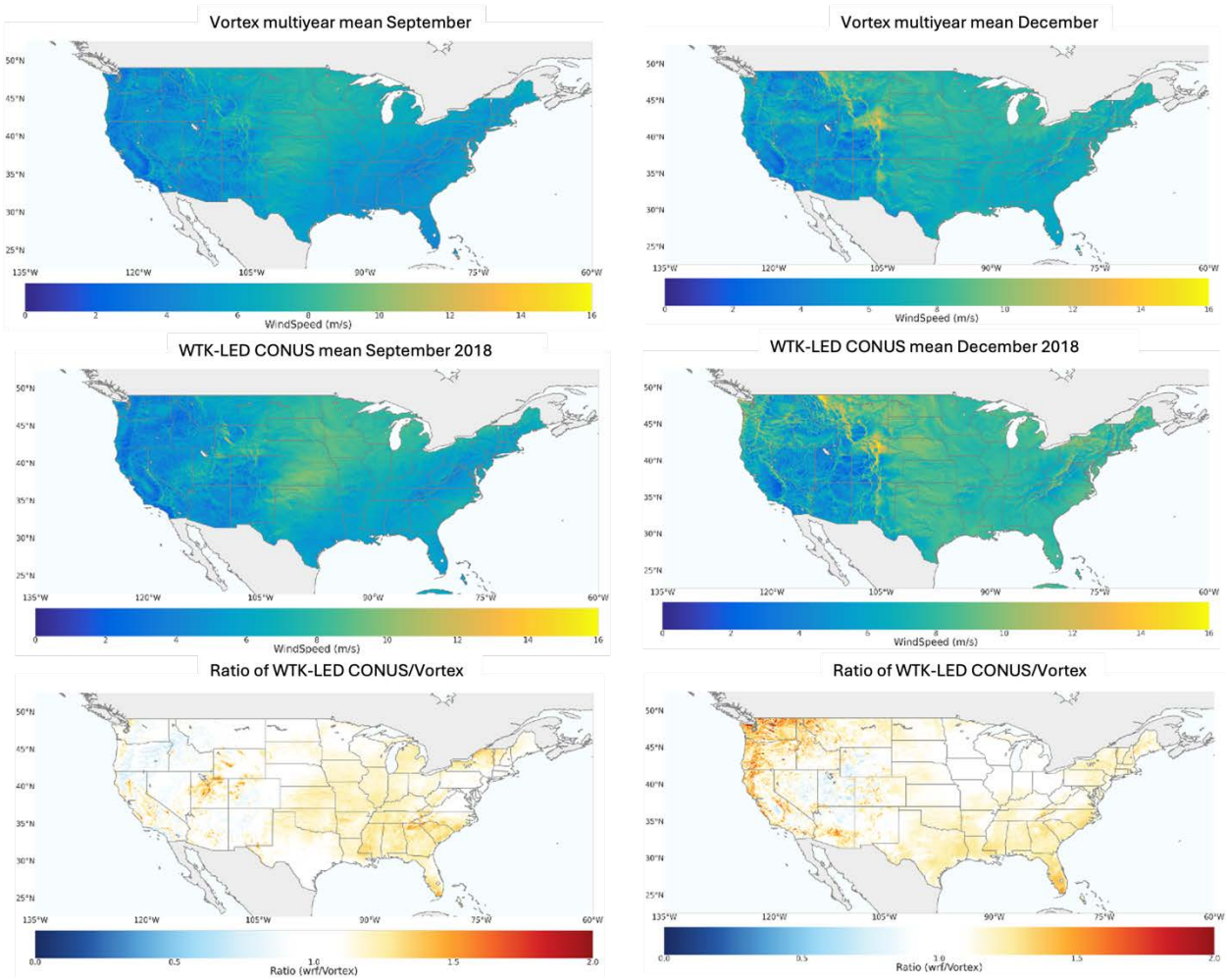

Figure 9. Comparison of 100-m wind speeds between WTK-LED CONUS simulated in 2018 and Vortex long-term mean The left column maps are for September, and the right column maps are for December. (Top) Vortex multiyear mean. (Middle) WTK-LED CONUS mean for 2018. (Bottom) Ratio of WTK-LED CONUS/Vortex data.

Figure 10 shows ratio maps similar to those in Figures 8 and 9, but for 2019 and 2020. In 2019, the 100-m wind speeds are slightly slower than the long-term mean from Vortex in March and June over the Northwest, but faster over the Southwest, Midwest, and especially the Southeast. The overestimation in the Southeast is common and is also seen in ERA5 because the wind speeds in this region are as low as the model's uncertainty and usually not fast enough to operate wind farms. Accurately capturing these winds is challenging. Since the benchmark data from Vortex has the same long-term mean used for Figure 8 and Figure 9, the differences between these maps for different years (2018, 2019, and 2020) indicate clear interannual variability in wind speeds. This interannual variability is usually larger than the uncertainty due to internal variability from initial conditions.

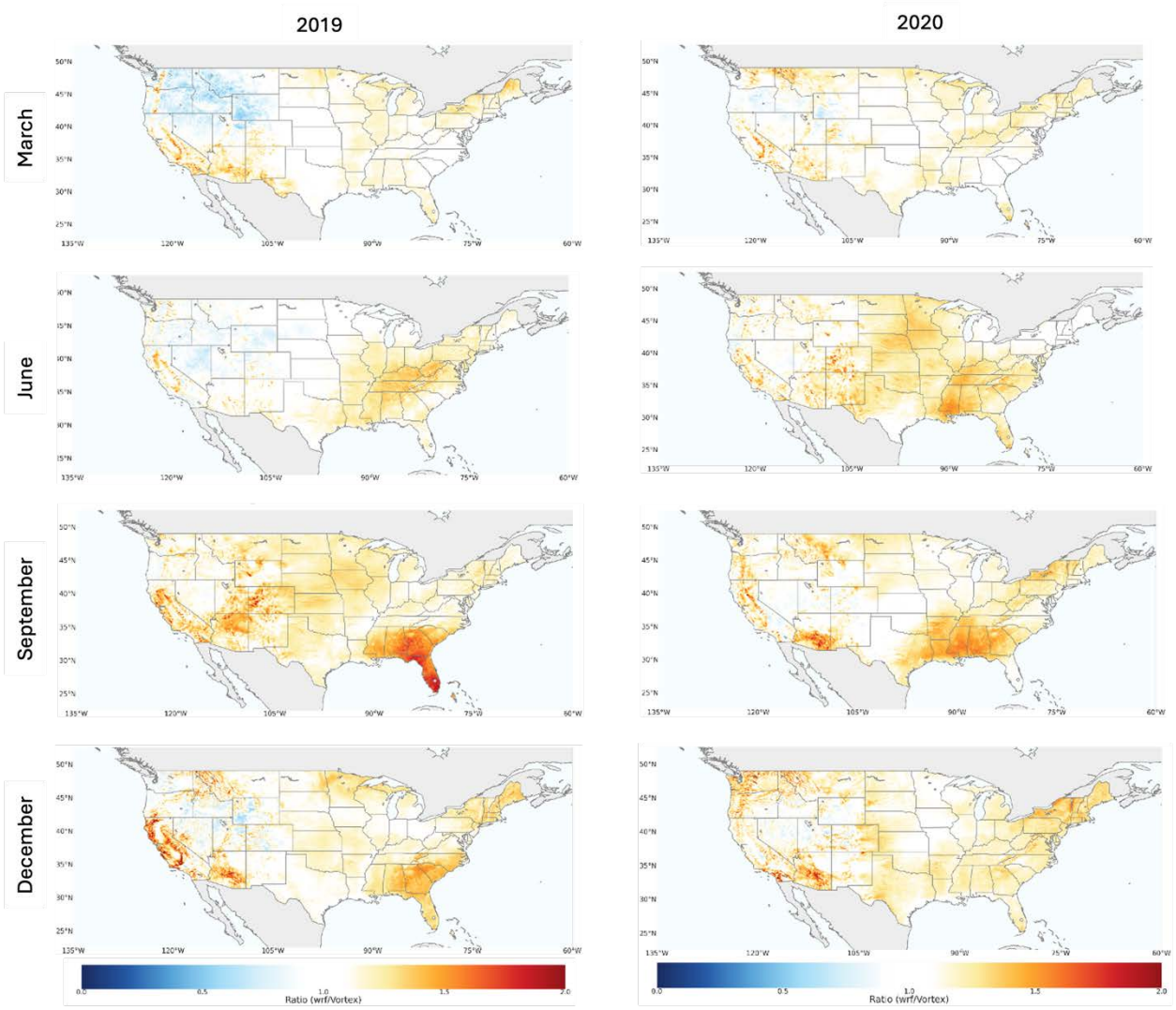

Figure 10. Ratio of 2-km WTK-LED CONUS/Vortex for (Row 1) March, (Row 2) June, (Row 3) September, and (Row 4) December. Left: ratio based on WTK-LED CONUS in 2019; right: ratio based on WTK-LED CONUS in 2020.

3.2 WTK-LED Alaska Validation

We present an observational validation analysis for the 5-min/2-km WTK-LED Alaska at several locations (Figure 11) and several measurement heights. The observations were from the National Data Buoy Center (n.d.) and the Alaska Energy Authority (n.d.).

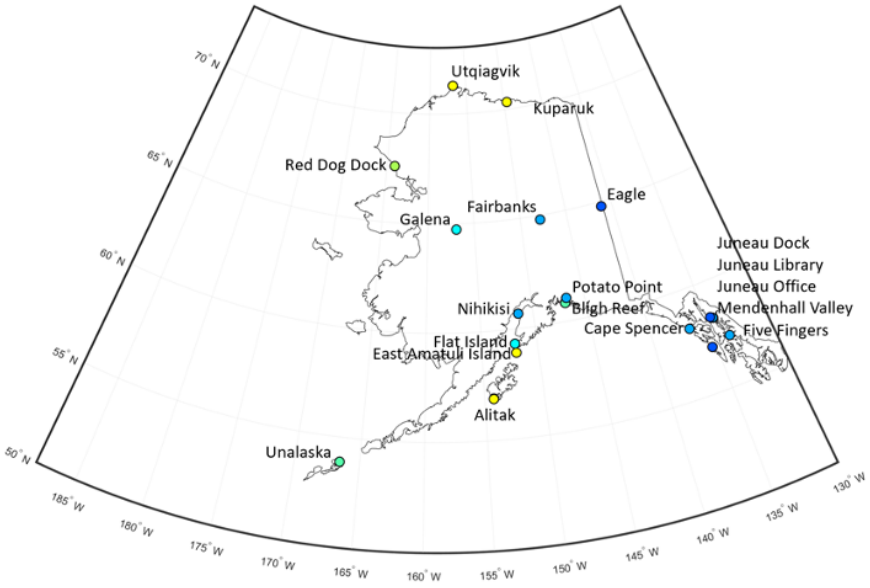

Figure 11. Location of measurements used to validate the WTK-LED over Alaska

At these sites, the wind speed bias was assessed during June and December of 2018 (Figure 12) for both the WTK-LED and ERA5 data to demonstrate a comparison with ERA5 as well. In June, the WTK-LED model simulations show a smaller bias magnitude at 11 sites, and ERA5 shows a smaller bias magnitude at 11 sites. For December, a smaller bias magnitude is shown at 12 sites for WTK-LED and at 10 sites for ERA5. The spatial distribution of the bias is shown in Figure 13.

Figure 14 and Figure 15 show the MAE: In June, the WTK-LED exhibits a smaller MAE at six sites, compared to ERA5, which shows a smaller MAE at 16 sites. For December, the WTK-LED has a smaller MAE at five sites compared to ERA5, which shows a smaller MAE at 17 sites.

Correlation values are better for ERA5 than for the WTK-LED (Figure 16 and Figure 17): The WTK-LED has a higher correlation at two sites, and ERA has a higher correlation at 20 sites for both June and December.

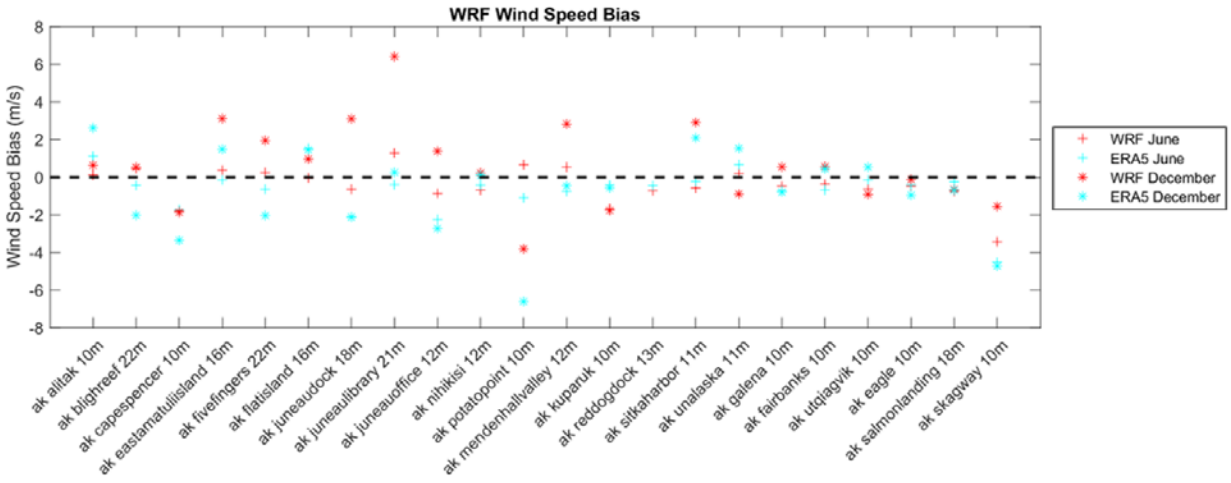

Figure 12. Wind speed bias (m/s) for the WTK-LED ("WRF") (red) and ERA5 data (cyan) at the observation locations used to validate the WTK-LED over Alaska

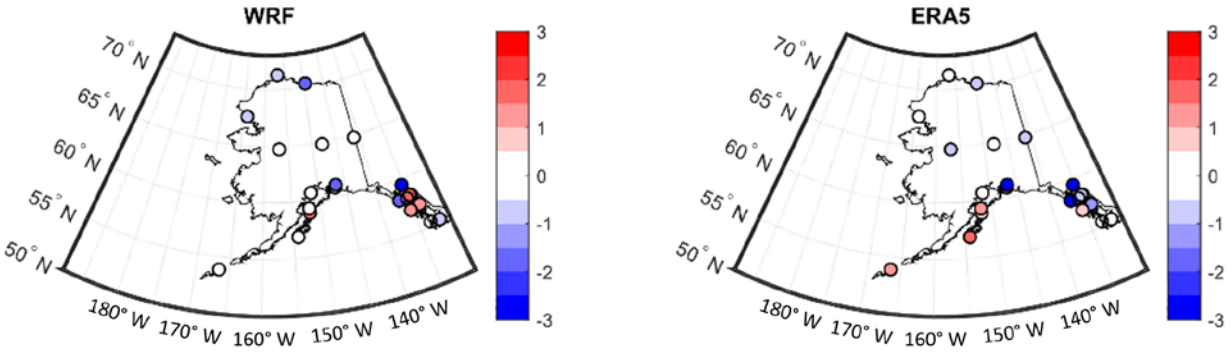

Figure 13. Wind speed bias (m/s) at various observation locations over Alaska for the (Left) WTK-LED ("WRF") and (Right) ERA5

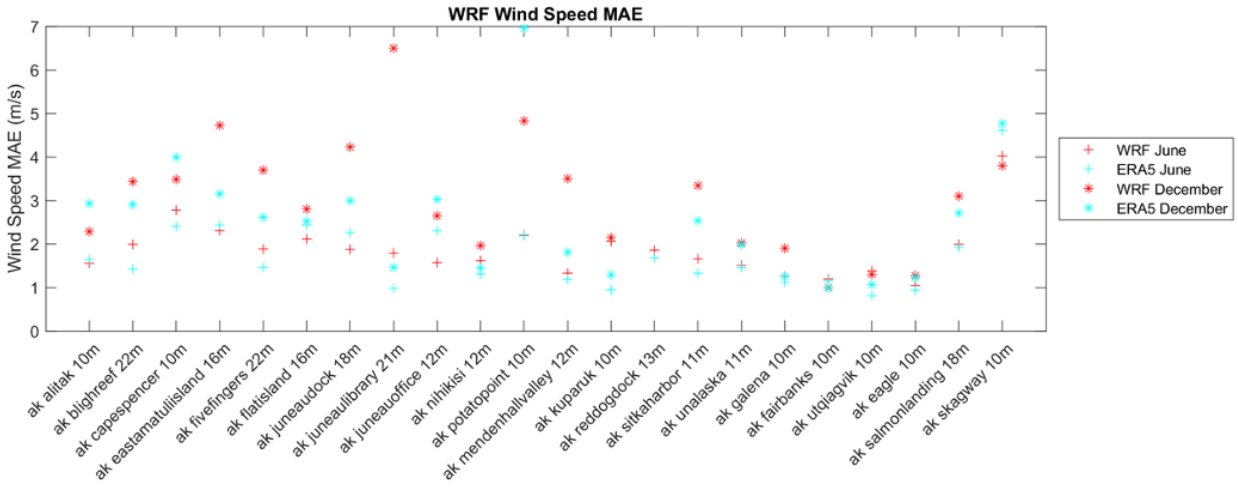

Figure 14. Wind speed MAE (m/s) for the WTK-LED ("WRF") (red) and ERA5 data (cyan) at the observation locations used to validate the WTK-LED over Alaska

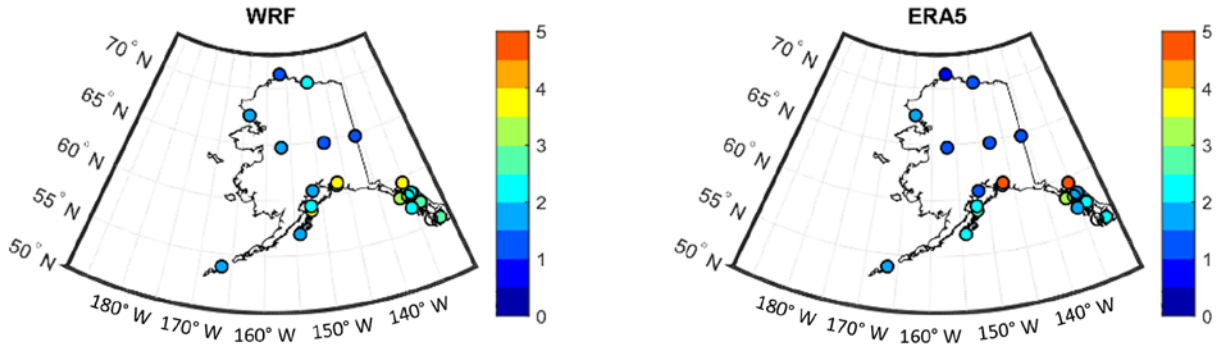

Figure 15. Wind speed MAE (m/s) at various observation locations over Alaska for the (Left) WTK-LED ("WRF") and (Right) ERA5

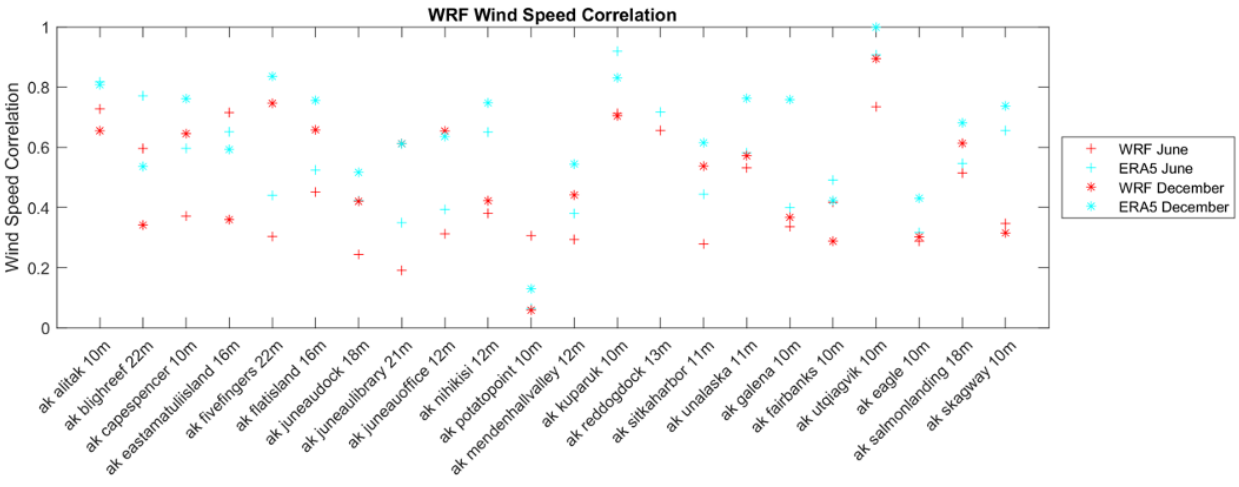

Figure 16. Wind speed correlation (m/s) for the WTK-LED ("WRF") (red) and ERA5 data (cyan) at the observation locations used to validate the WTK-LED over Alaska

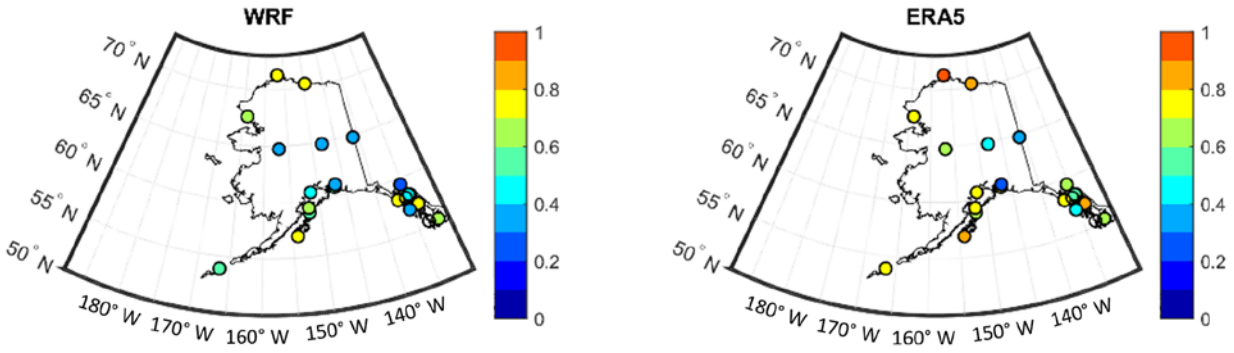

Figure 17. Wind speed correlation at various observation locations over Alaska for the (Left) WTK-LED ("WRF") and (Right) ERA5

Additionally, a comparison analysis was performed with WTK-LED Alaska and Vortex data (Figure 18). Depending on the month and location, the ratio of WTK-LED Alaska/Vortex data can reach up to 2.

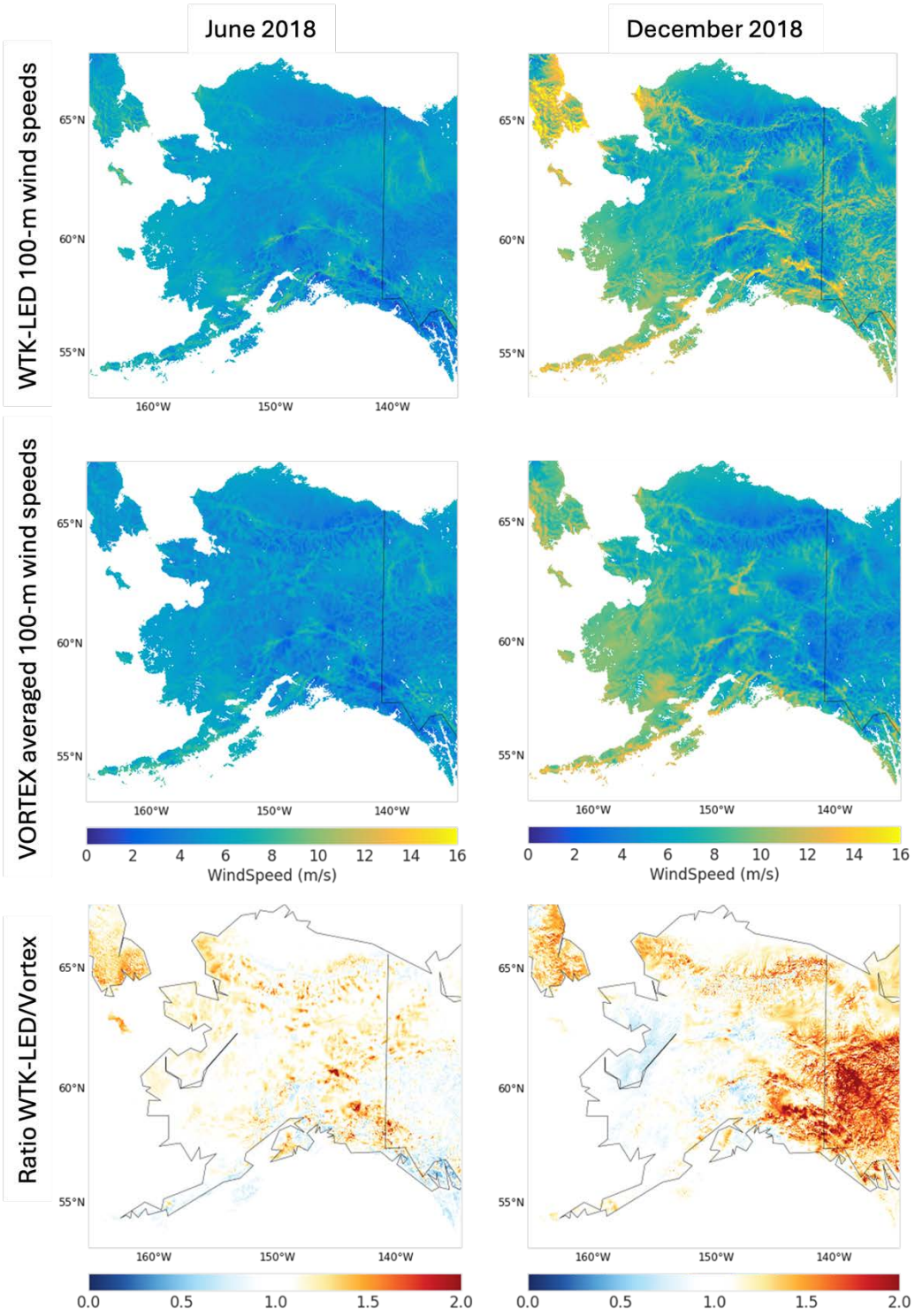

Figure 18. (Row 1) WTK-LED wind speed simulations at 100 m averaged over June 2018 (left) and December 2018 (right). (Row 2) VORTEX long-term averaged wind speeds at 100 m averaged over all months of June from 2001 to 2020 (left) and over all months of December from 2001 to 2020 (right). (Row 3) Ratio between WTK-LED and VORTEX.

3.3 WTK-LED Hawaii Validation

We compared the WTK-LED Hawaii simulations with those produced and published by the University of Hawaii (UH) available at https://www.pacioos.hawaii.edu/weather/model-wind-mauioahu/#access. The WTK-LED model domain covers the entire island chain, whereas the domain from UH only covers part of the islands. Therefore, we compare the simulations only for the overlapping domain (Figure 19). Because we do not have any observations to validate the results, we do not assess the accuracy of the model simulations but use the simulations from UH as a reference to judge if the WTK-LED produces reasonable results over Hawaii. Note also that the UH simulations are hourly forecasts and not hindcasts like the WTK-LED.

While the WTK-LED over Hawaii exhibits higher wind speeds than UH's dataset, the WTK-LED captures similar spatial patterns and seasonal variability (there is not much difference in wind speeds and directions between different seasons). Wind speeds are generally lower over the islands than over the ocean. There are some localized changes in wind speeds over the islands, indicating there are local structures that affect the wind speeds.

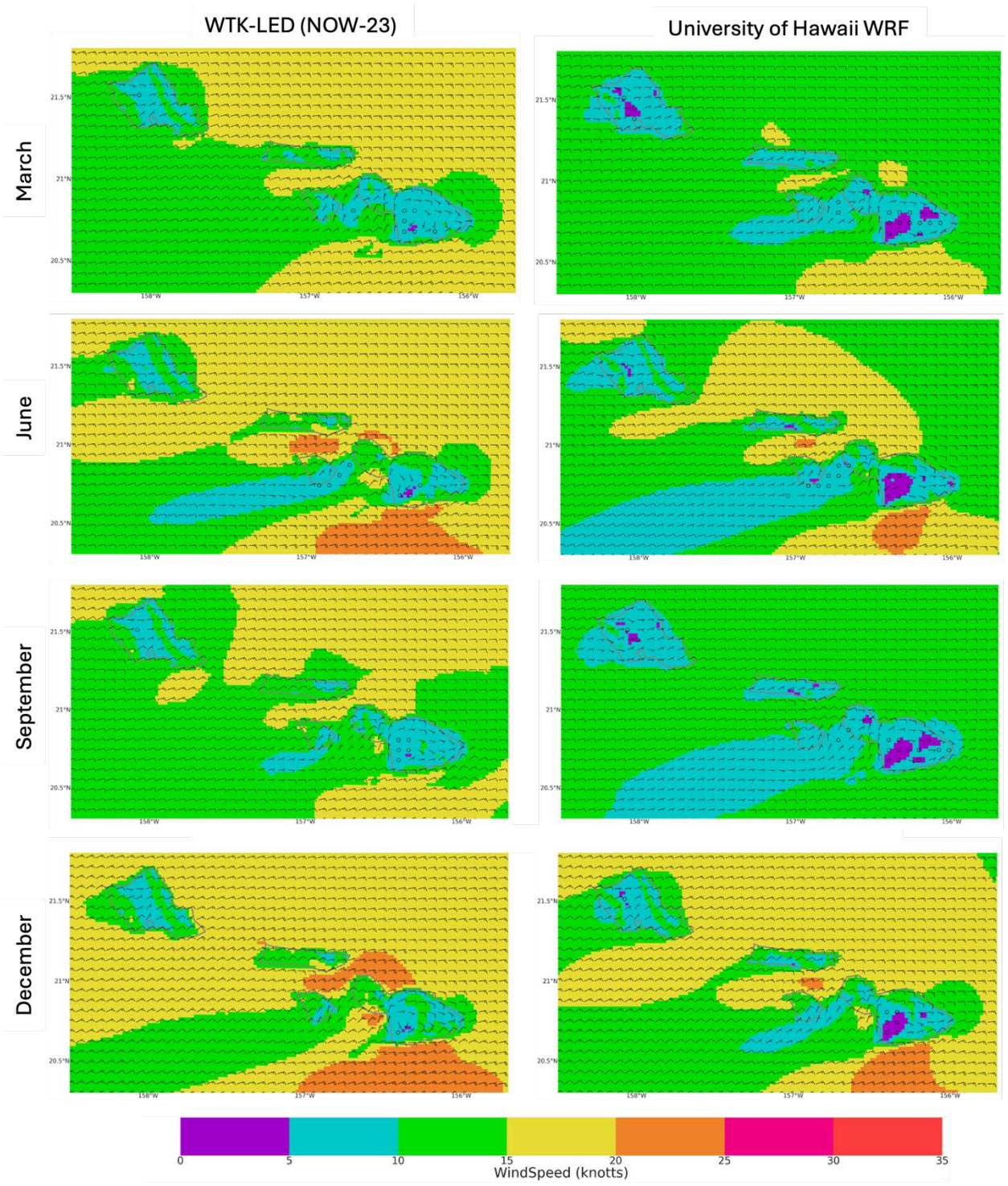

Figure 19. 10-m wind speed comparison between (Left) WTK-LED simulations and (Right) University of Hawaii's 2-km WRF simulation, in (Row 1) March, (Row 2) June, (Row 3) September, and (Row 4) December. Note that the units in these maps are knots.

We have also computed island-wide averages using hourly wind speeds for three major Hawaiian islands. Their diurnal cycles and probability density functions (PDFs) in each month are shown in Figure 20. We found that winds simulated by WTK-LED are higher than those simulated by UH, but the diurnal patterns are very similar. The overlap of PDFs between two datasets are mostly larger than 70%, indicating similar distributions, except that the WTK-LED has a larger mean and median value.

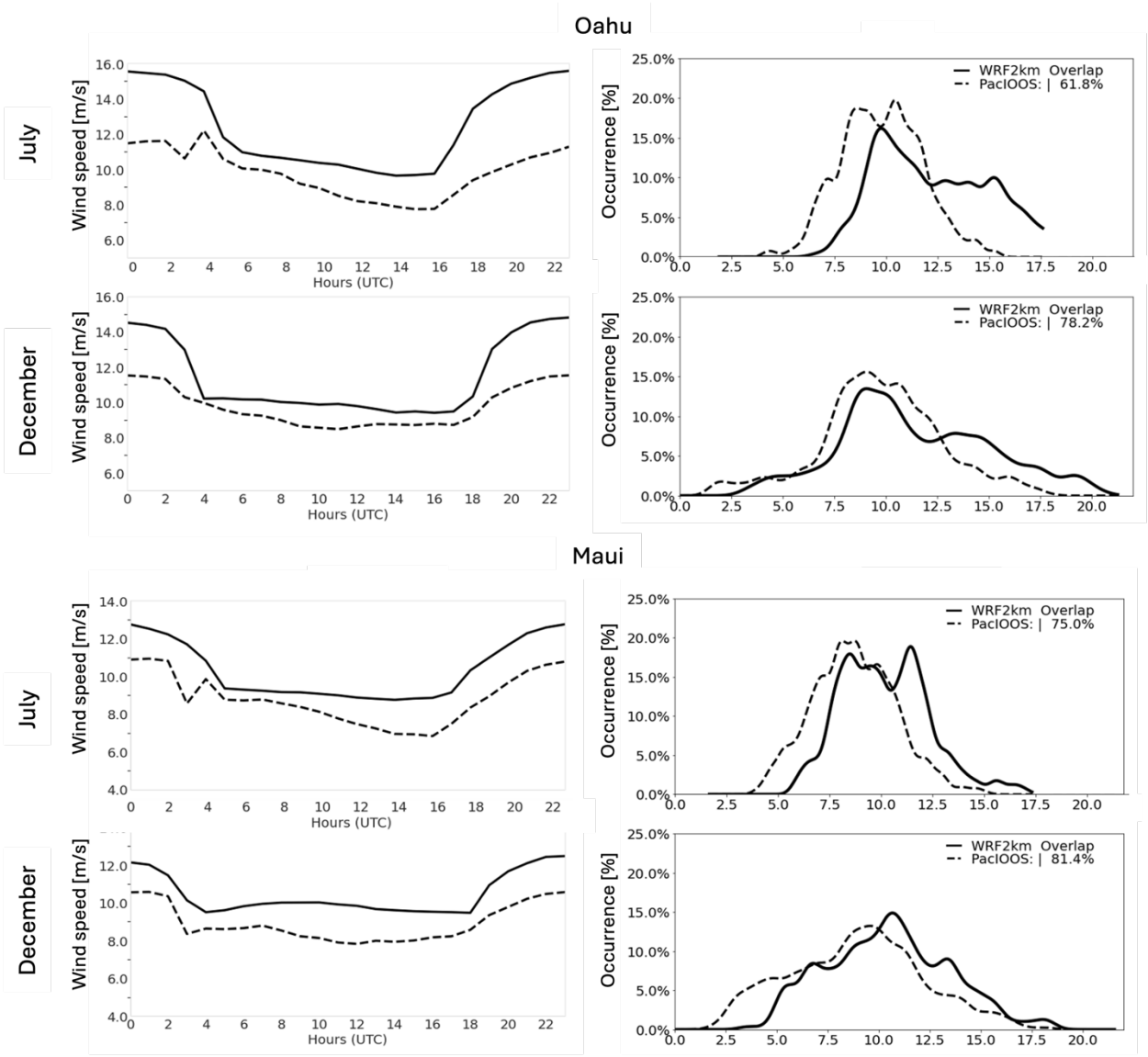

Figure 20. Comparison of diurnal cycles of island-wide averaged hourly wind speeds for July and December. Top two rows: Oahu, HI. Bottom two rows: Maui, HI. Left column: averaged diurnal cycle. Right column: probability density function of wind speeds.

3.4 WTK-LED Climate Validation

We conducted preliminary validation of the WTK-LED Climate dataset at 4-km grid spacing and hourly intervals by comparing simulations to observations at various heights (Validation sites are shown in Figure 21). A more comprehensive validation will be presented in a forthcoming paper by Wang et al.

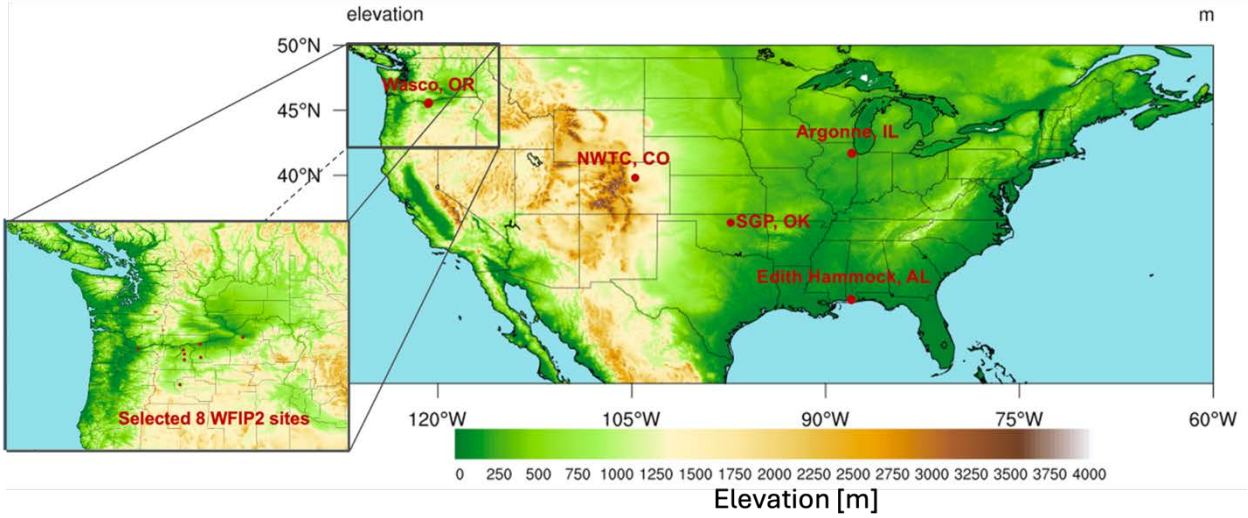

Figure 21. Map showing the selected observation sites across the contiguous United States. The inset shows eight sites from the Second Wind Forecast Improvement Project (WFIP2) in the northwestern United States that were evaluated.

Climate-scale simulations are meant to capture climatological statistics (e.g., mean, variance, maxima, minima). Our validation focuses on these aspects in Figure 22 showing PDFs over various terrain conditions. From this analysis, we conclude that WTK-LED Climate matches the observed PDFs reasonably well at most sites, even in complex terrain, although it overestimates wind speeds in some regions (e.g., southeastern United States). ERA5 performs well over relatively flat regions but struggles in complex terrain, with overestimations of low wind speeds and underestimations of high wind speeds, especially over mountains.

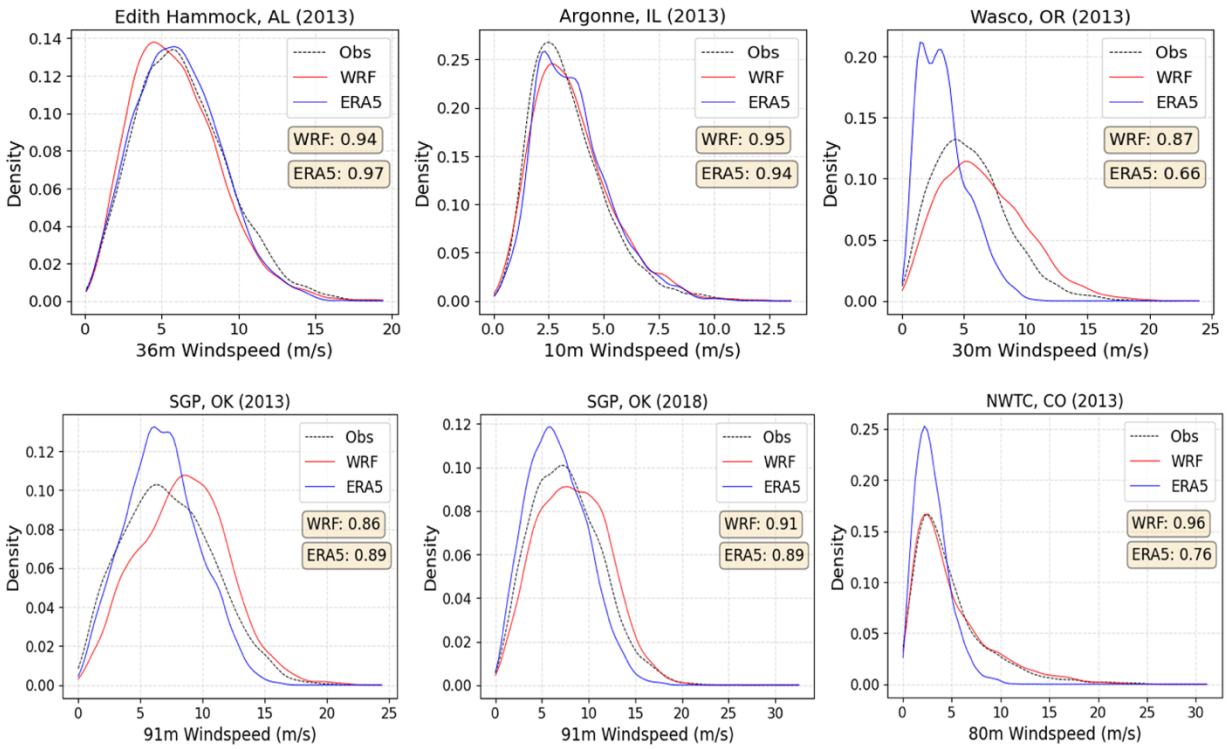

Figure 22. Observed, WTK-LED Climate, and ERA5 simulated PDFs of wind speeds at various sites and heights for 2013 and 2018. The overlapping ratio is indicated in the boxes for WTK-LED Climate (WRF simulations) and ERA5; the closer to 1, the better.

Next, we evaluate the seasonally averaged diurnal cycle of wind speeds and seasonally averaged wind roses (Figure 23 and Figure 24). It is interesting to note that the performance of the WTK-LED Climate simulations varies depending on the season and site. We use one of the sites at the Atmospheric Radiation Measurement user facility in Oklahoma, as many of the model physics parameterizations, including the radiative transfer model, were calibrated based on this site. While it is encouraging to see that the WTK-LED Climate data performs reasonably well at this site for both diurnal cycles in wind speeds and wind roses, we see different biases across various locations. In general, consistent with the PDFs, the model performs better over complex terrain than ERA5 and shows overestimations in flat regions. Wind directions are generally captured at all sites. These findings indicate that the WTK-LED Climate captures the main physics that govern the winds.

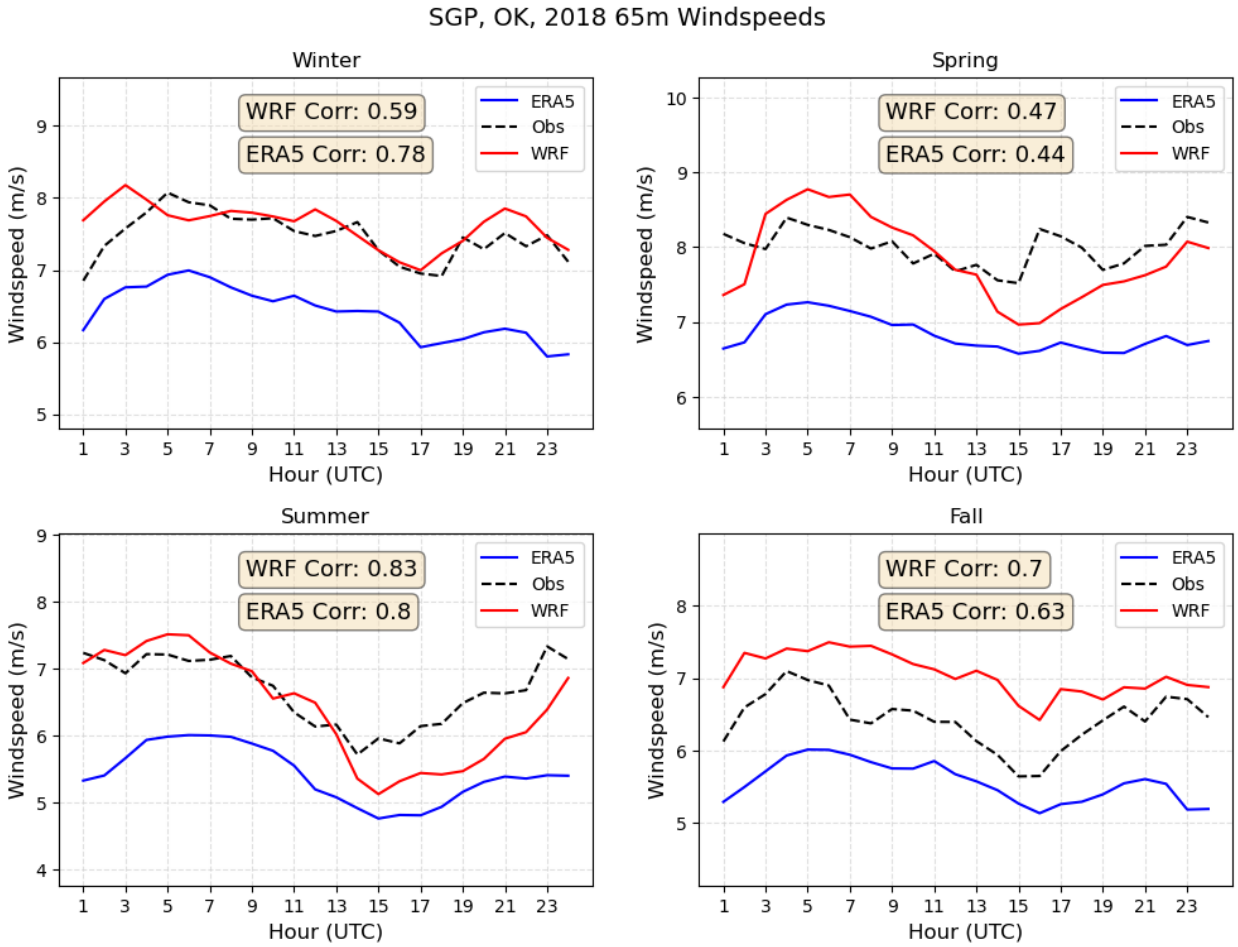

Figure 23. Averaged diurnal cycle of wind speeds at 65 m at the Southern Great Plains site in Oklahoma for ERA5, WTK-LED Climate (WRF), and observations for winter, spring, summer, and fall. The correlation is indicated in the boxes for WTK-LED Climate (WRF simulations) and ERA5.

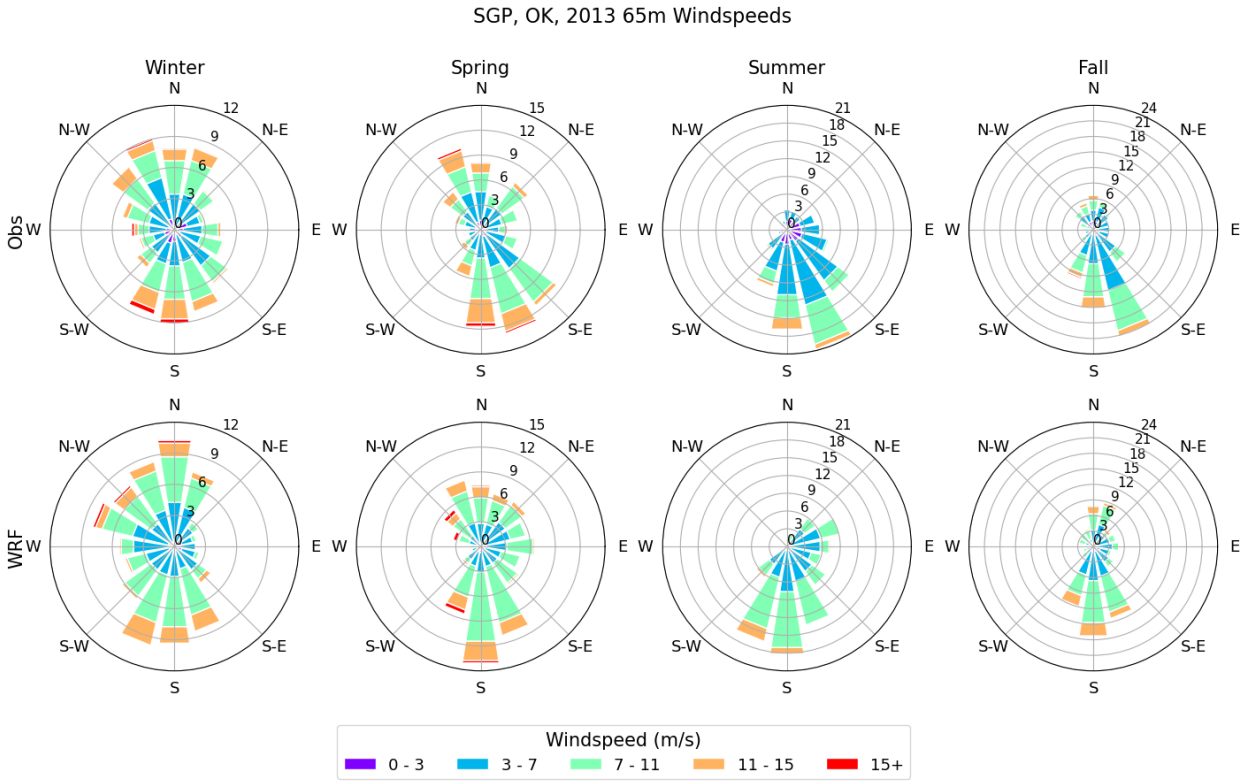

Figure 24. Wind roses for 65-m wind speeds at the Southern Great Plains site in Oklahoma for (bottom row) WTK-LED Climate (WRF), and (top row) observations for winter, spring, summer, and fall

Hour-to-hour variability is important for certain grid integration applications; therefore, we show the day-to-day variability of wind speeds in the WTK-LED Climate data at one specific location (Figure 25) as an example. We see that the simulations can capture peaks and the general characteristics of the flow, but often at different times than observed, resulting in poor data correlation (0.25). This bears the question: At what timescale do the WTK-LED Climate data depict the flow pattern accurately enough for various applications? In Figure 26 we therefore show RMSE and correlation at various sites for daily, weekly, biweekly, and monthly averages. As we average the data over longer timescales, the correlation increases, and the RMSE decreases at all but one site (Wasco, Oregon, with complex terrain). While these results are expected from a climate science perspective — showing performance with correlations close to 0.9 and relative RMSE around 10% is considered decent in climate models — they should not be used for capturing hour-to-hour variability needed for grid integration applications.

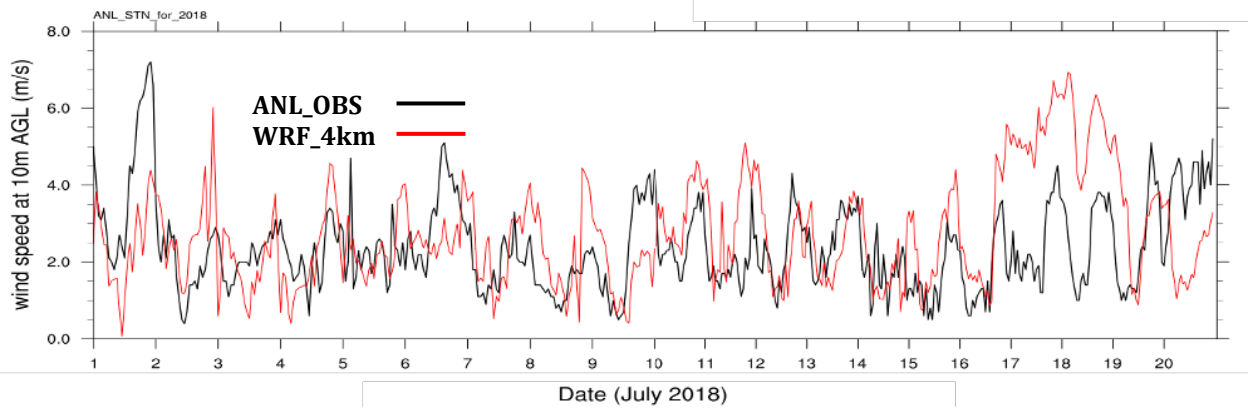

Figure 25. Hour-to-hour variability of 10-m wind speed above ground level (AGL) (m/s) at the Argonne observation station in the first 20 days of July 2018. Observations are in black, and 4-km WTK-LED Climate simulations in red. The correlation has been calculated to be 0.25 for this time period.

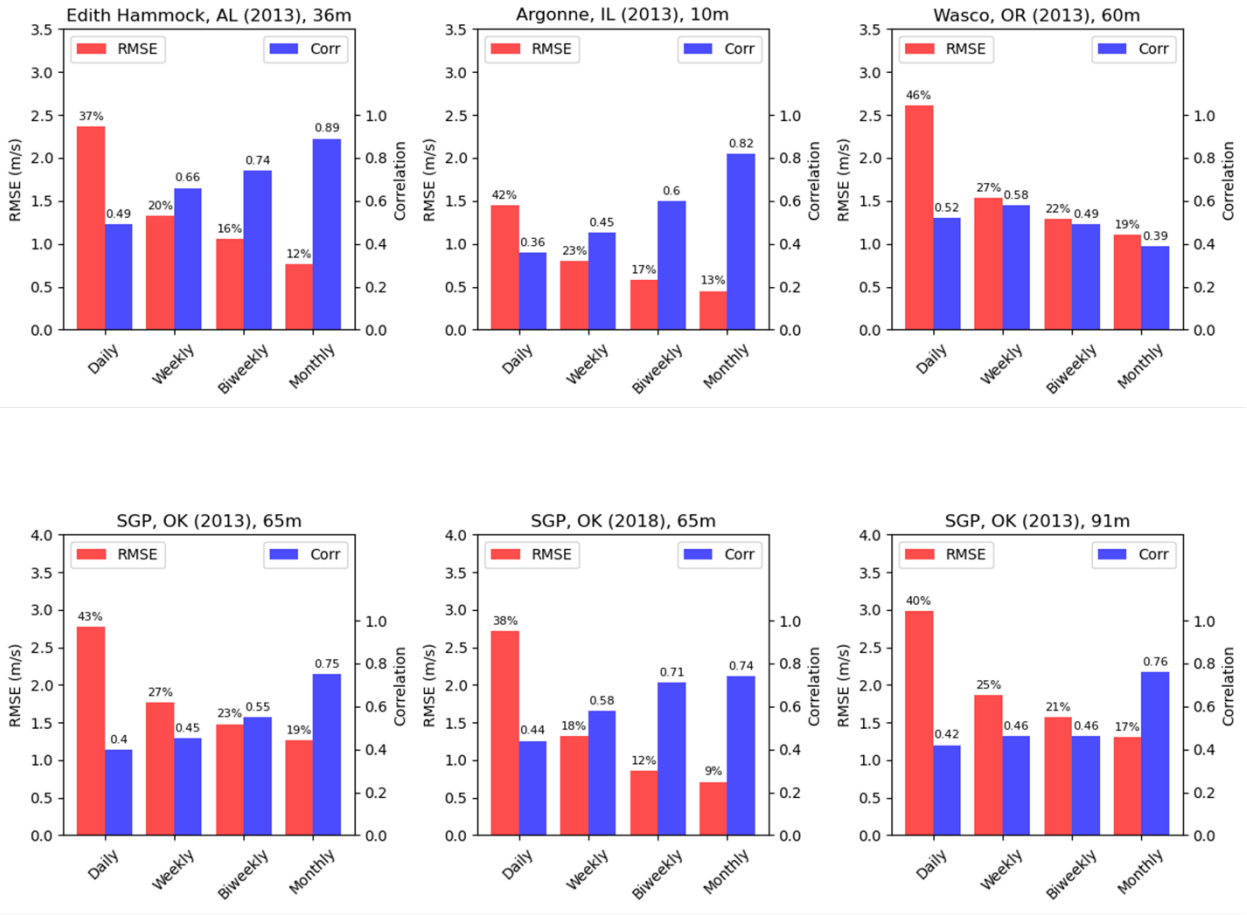

Figure 26. Relative RMSEs (red) and correlation (blue) of simulated wind speeds at various sites and heights for the year as indicated in the panel titles. The relative RMSE is calculated using RMSE divided by the observed annual mean wind speeds.

4 Uncertainty Quantification

For all the wind datasets and validation presented in this report and for publicly available wind data products, including WIND Toolkit, Global Atlas Vortex, and HRRR, the data are created deterministically. This means the potential range of the data is not shown if the model is run using different physics or is initialized from a different day or hour. At locations with high wind speeds, the uncertainty can also be high, whereas at locations with slightly lower wind speeds, the uncertainty can be low. Wind farm planners need this information to better inform siting decisions and avoid regions with high uncertainties and large variabilities in wind energy potential. To address this need, ensembles were set up to estimate wind speed model uncertainty for CONUS, Alaska, and Hawaii, accounting for both model structural uncertainty and uncertainty due to internal variability. We describe how model uncertainty was deduced from these ensembles. Quantifying this uncertainty is crucial for providing accurate assessments of the confidence surrounding the deterministic wind speeds used to assess wind resources at different locations. Note that we are not estimating the uncertainty that arises from comparing model simulations with real-world observations.

4.1 Sensitivity of Uncertainty Estimation to Ensemble Size

As described in Section 2.2.3, we conducted 24 ensemble runs for the WTK-LED Alaska setup, which allows us to study the sensitivity of ensemble size uncertainty estimation. A statistical bootstrapping (a resampling) technique is applied to the 24 runs in December along the hourly time dimension (744 time steps in each December) to produce a sample pool with 500 augmented Decembers. Augmented Decembers still have 744 time steps per month and maintain temporal dependence but are generated by selecting wind speeds at each time step that may come from any of the 24 runs. That is, an individual sample is produced when one of the data points (24×744) is randomly selected to create a new time series for 100-m wind speeds (Figure 27). Each resampled time series is the same size as the original data—744 time points in December at hourly intervals. The augmented sample pool of ensemble members is used to represent a range of wind speeds created by considering both uncertainty sources. To cover that wind speed range, we can take medians (50th percentile), upper bounds (97.5th percentile), and lower bounds (2.5th percentile) from the 500×744 wind speed sample pool.

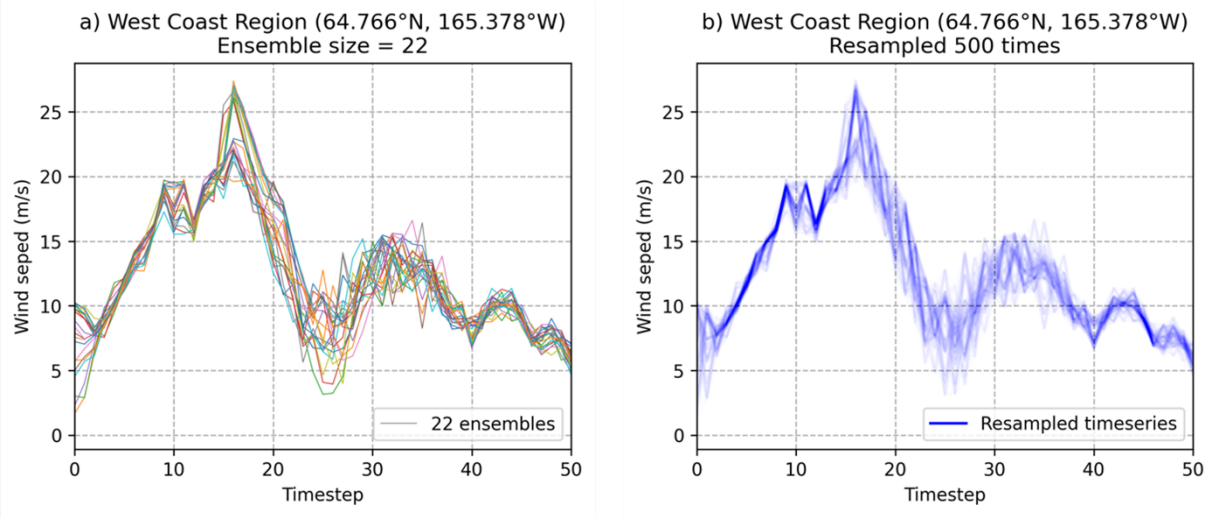

Figure 27. Statistical resampling demonstration with (a) 22 original ensembles and (b) those 22 ensembles resampled 500 times to produce a large, augmented time series with the same time-dependence as the original ensembles. Uncertainty calculated on 500 resampled time series provides more robust characterization of ensemble variability than on the original pool.

To investigate the minimum ensemble size required for a robust estimation of wind speed uncertainty or to examine whether the 24 members are sufficient for covering the uncertainty range of wind speeds, we can estimate the 5th, 50th, and 95th percentiles based on bootstrapping different numbers of ensemble runs. For example, we start with selecting two ensemble members randomly from the 24-member ensemble, then carry out a series of bootstrapping experiments by progressively increasing the ensemble size (Alexandru, de Elía, and Laprise 2007). We made sure that the chosen ensemble members always include both uncertainty sources. If a quantity of interest (e.g., 50th percentile) converges to a very small variability in wind speed when we reach a certain ensemble size, that means the ensemble size is sufficient to cover both uncertainty sources studied here. Note that this bootstrapping approach can incorporate more uncertainty sources, such as parameter uncertainty, forcing data uncertainty, and others if the ensemble is available.

Figure 28 demonstrates that small ensemble sizes generate a large spread of model variability estimates without capturing the full magnitude of variability. Five members generally capture the full magnitude of variability (with the exception of the Southeast Coast Region), but may still underestimate the variability depending on which ensembles are randomly sampled. Good agreement for ensemble sizes greater than 12 indicates the ability to generate a robust assessment of wind speed variability considering both structural and internal variability. This means that, even if we included more than our 16 ensemble runs, we expect the variability of the model simulated wind speed would not significantly change. This is an encouraging finding, because running more ensemble members requires a large amount of computational resources and storage space.

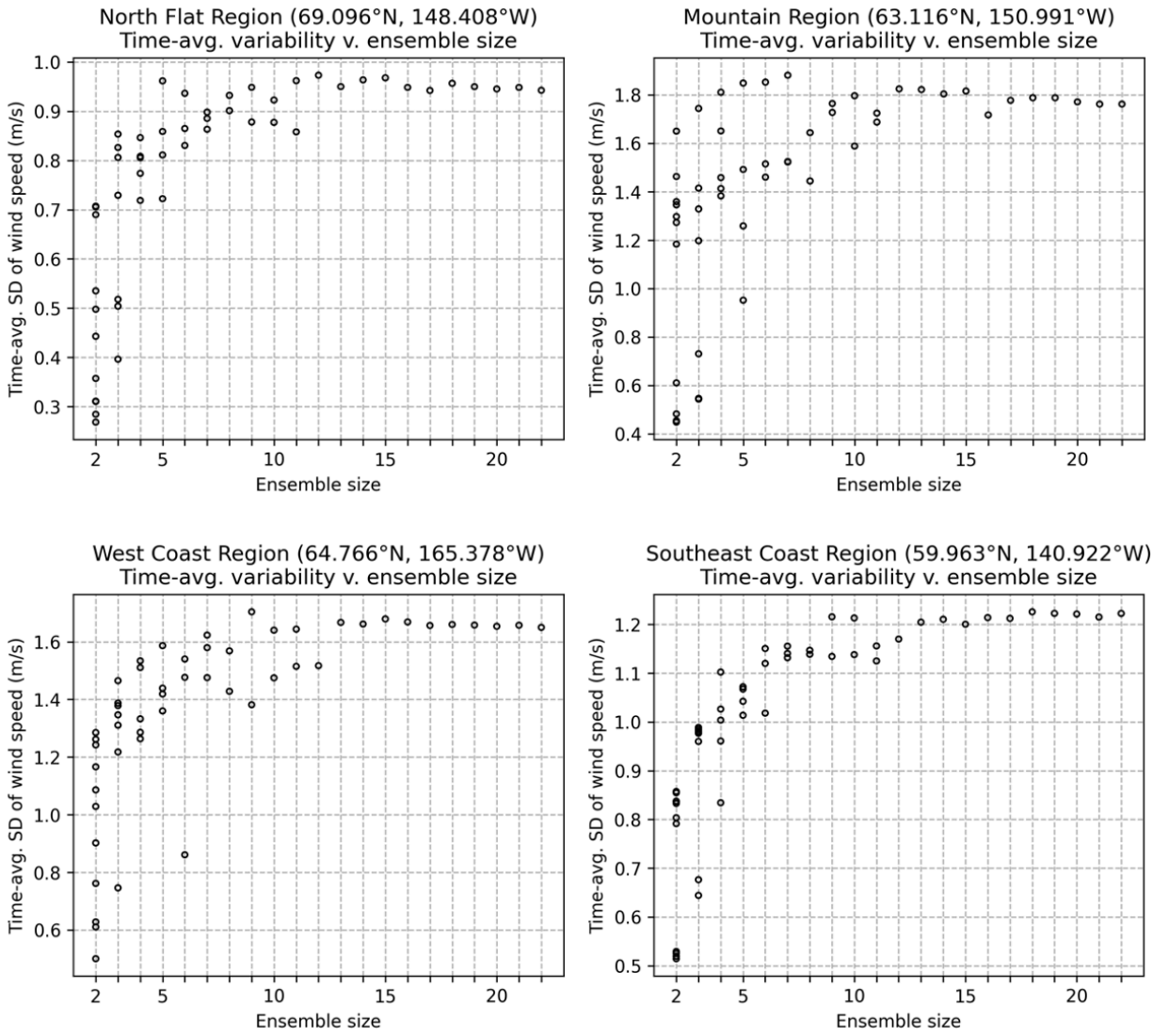

Figure 28. Ensemble-size experiment over four locations in Alaska indicated by the latitudes and longitudes: variation of the 100-m wind speeds created by ensembles considering both internal variability and structural uncertainty, with the ensemble size from 2 to 20, randomly sampled from the 24 members. Note that the variability on the y-axis is averaged across time (744 time points). The variability at hourly scale (without averaging) is much larger than shown.

4.2 Expressing the Uncertainty

After confirming that the 16 ensemble members (10 representing structural uncertainty and 6 representing internal variability) are sufficient, we performed statistical bootstrapping on the ensemble runs. This process generated 500 augmented ensemble members, each with the same spatial and temporal domain as one of the original 16 ensemble members. Subsequent analysis took different time averages across the 500 ensemble members, including daily averages, weekly averages, biweekly averages, and daytime and nighttime averages for the entire month. For the daytime and nighttime averages, we averaged every 21 UTC (daytime) and 06 UTC (nighttime) across all 31 days of January. Once the averages were calculated, we determined the percentiles (5th, 25th, 50th, 75th, and 95th) across the 500 ensemble members for every spatial grid point and time step. This helped us analyze the degree of spread between the upper and lower bounds of the 100-m wind speeds. The range between the 5th and 95th percentiles from the 500 ensemble members ultimately represents the uncertainty in the wind speeds over a certain location across the domains covered by all WTK-LED simulations.

Figure 29 shows the resulting uncertainties of 100-m wind speeds using the method described above for the WTK-LED Climate data over North America for January 2018. Here, we present weekly and biweekly timescales. For each timescale, a random time step (e.g., a certain week or a certain day) was chosen to plot the maps in the figure. Intuitively, the magnitude of the uncertainties scales with the resolution of the temporal averages. The biweekly uncertainties mostly fall within the range of 0.3–0.7 m/s across the contiguous United States, with higher uncertainties over the Rockies, Great Lakes and Northeast. The weekly uncertainties are notably higher, ranging mostly between 0.5 and 1.2 m/s. The daily average, at the highest temporal resolution used in this analysis, shows the highest uncertainties across the spatial domain, with most values exceeding 2.5 m/s, especially in regions where the wind speed itself is low, such as in the western and southern United States. This means that if the model simulations are conducted using different physics parameterizations or initial conditions, the output can vary significantly, with differences as large as the wind speeds at these locations. This also indicates that the numerical models are not capable of accurately simulating very low wind speeds, which often fall within the range of model uncertainty. Fortunately, the wind farms do not operate until wind speeds reach 4–5 m/s, so this limitation has minimal impact on operational decisions.

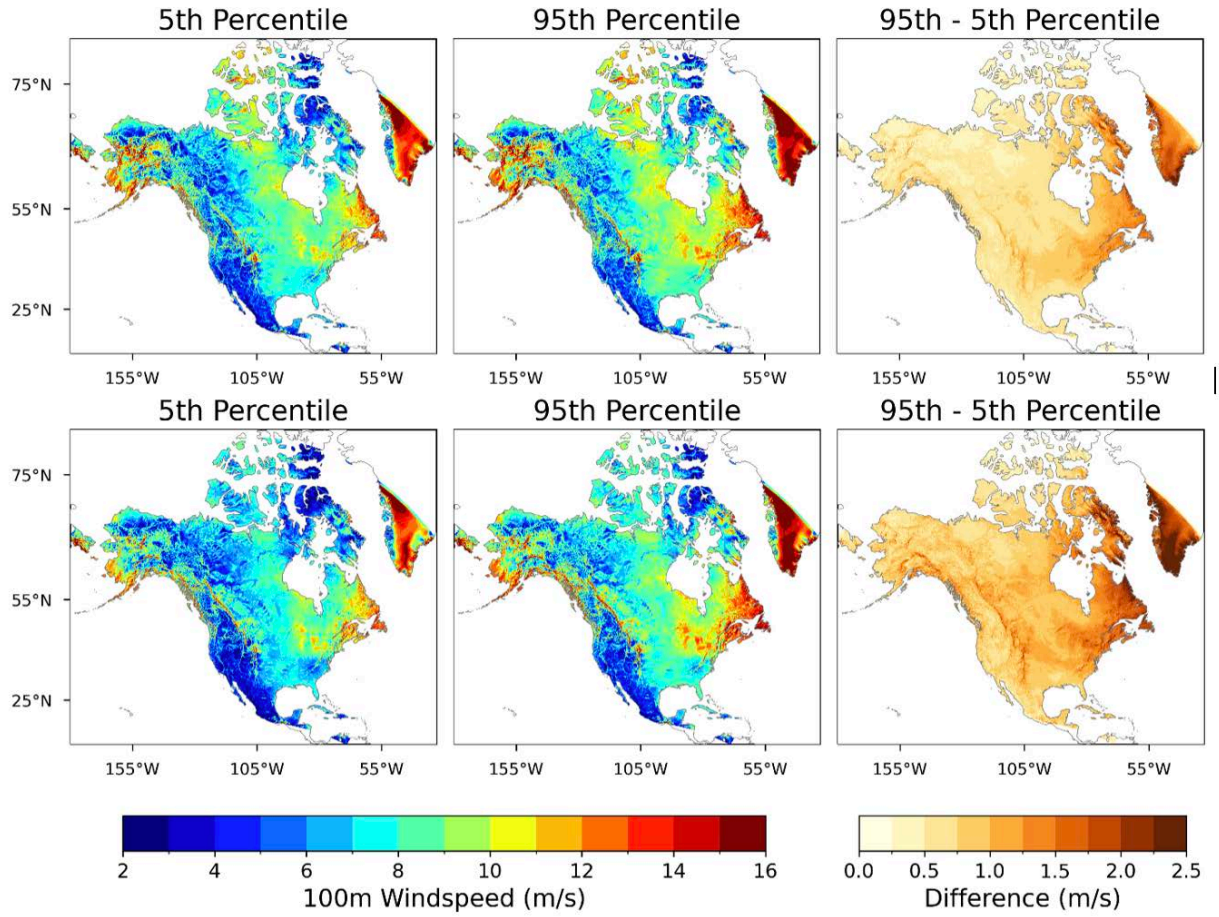

Figure 29. 5th percentile, 95th percentile, and 95th minus 5th percentile taken across the 500 resampled ensembles at the biweekly (1st row) and weekly (2nd row) averaged timescale

Figure 30 shows an example of uncertainty in August 2018 over the Hawaiian Islands and the surrounding Pacific Ocean. Presented here are the nighttime and daytime monthly averaged 100-m wind speeds. Note that both daytime and nighttime are represented by only one hour, resulting in a relatively large uncertainty compared to monthly or biweekly mean wind speeds. Summer has the highest wind speeds due to persistent trade winds blowing in from the northeast. In contrast, winter winds can come from any direction and may also yield high winds, but not as persistently strong as in summer. We can see that in August, and summer in general, wind uncertainty over the upwind side (east coast) is smaller than over the downwind side (west coast). Once the winds pass through the islands and are influenced by terrain effect, the model uncertainty becomes larger.

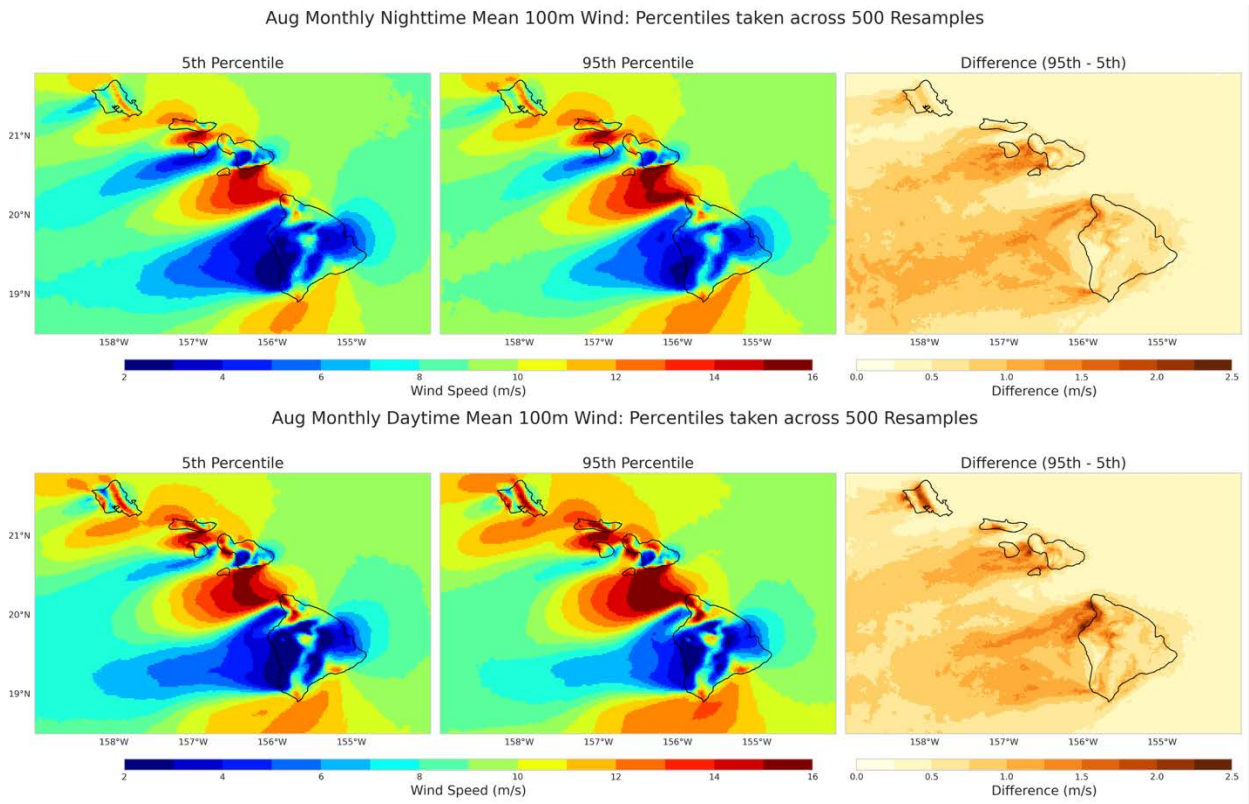

Figure 30. 5th percentile, 95th percentile, and 95th minus 5th percentile taken across the 500 resampled ensembles at the daytime and nighttime monthly averaged timescale in the month of August.

5 WTK-LED Dissemination and Public Access

The WTK-LED data are licensed for public use using a modified three-clause Berkeley Software Distribution open-source data license and indexed in key public data repositories such as OpenEI and Data.gov. The data, while large, are made available using several different systems to suit different users' needs, as described in the subsequent sections.

5.1 Data Format and HPC Access

After postprocessing, the WTK-LED data are stored in HDF5 files on NREL's Kestrel high-performance computing system. These files are available on a high-performance file system to all researchers and users of this system. The resulting files sizes per year are shown in Table 6.

Table 6. Annual Dataset File Information

Dataset	Individual Size (terabytes)	Number of Files	Total Size (terabytes)
Alaska, 5-min/2-km[a]	~0.68	15	9.9
Alaska, hourly	2.4	1	2.4
CONUS, 5-min/2-km[a]	~2.8	15	36
CONUS, hourly	5.8	1	5.8
North America Climate	3	1	3

[a] The 5-min files are stored as separate files per available height.

5.2 Scalable Data Platform

To support dissemination of this large data resource to various tools and platforms, the WTK-LED uses the same system for data dissemination pioneered by the original WIND Toolkit. This system leverages the HDF Group's Highly Scalable Data System (HSDS) and the Amazon computational cloud Simple Storage Service and Elastic Cloud Compute (Phillips et al. 2024). This system has several key benefits:

1. As a member of Amazon's Public Data Initiative (Amazon Sustainability Data Initiative, n.d.), the WTK-LED is available free of charge. This means no access or egress fees for data requests to the Simple Storage Service platform.
2. The HSDS service, running on Amazon Elastic Cloud Compute, is able to subset the files stored in their native HDF5 format, allowing users to select just the values or subsets of values needed from the source data. A public instance allows users to do this for free, and the open-source nature of the design means individual users can also deploy their own HSDS instance for arbitrary scalability.
3. Finally, the API Umbrella framework (https://github.com/NREL/api-umbrella) and infrastructure at api.data.gov allow for controlled access to the public HSDS service, preventing misuse or abuse while not preventing those users needing access to the full data to do so through Simple Storage Service.

In addition to this platform, ongoing work is evaluating additional serverless frameworks that can support very high volumes of queries, e.g., for public API access not needing rate limiting or control.

5.3 Web Platform

The WTK-LED is available in NREL's Wind Resource Database (WRDB), an interactive web platform, at https://wrdb.nrel.gov (Figure 31). Postprocessed data are available from the 4-km North America domain, the 2-km CONUS and Alaska domains, and over Hawaii. The WRDB is a collection of modeled wind resource estimates not only for the United States but also for various countries around the globe. The web-based platform allows the user to view and download datasets over various countries at various spatial and temporal resolutions. For the 20-year climate data over North America as well as the Hawaii and Alaska simulations, uncertainty estimates will be provided in the future. The available meteorological variables are listed in Table 7.

In addition to the WRDB, the WTK-LED data will be available on OpenEI (https://data.openei.org/submissions/2) and can be accessed via an AWS Public Dataset Bucket.

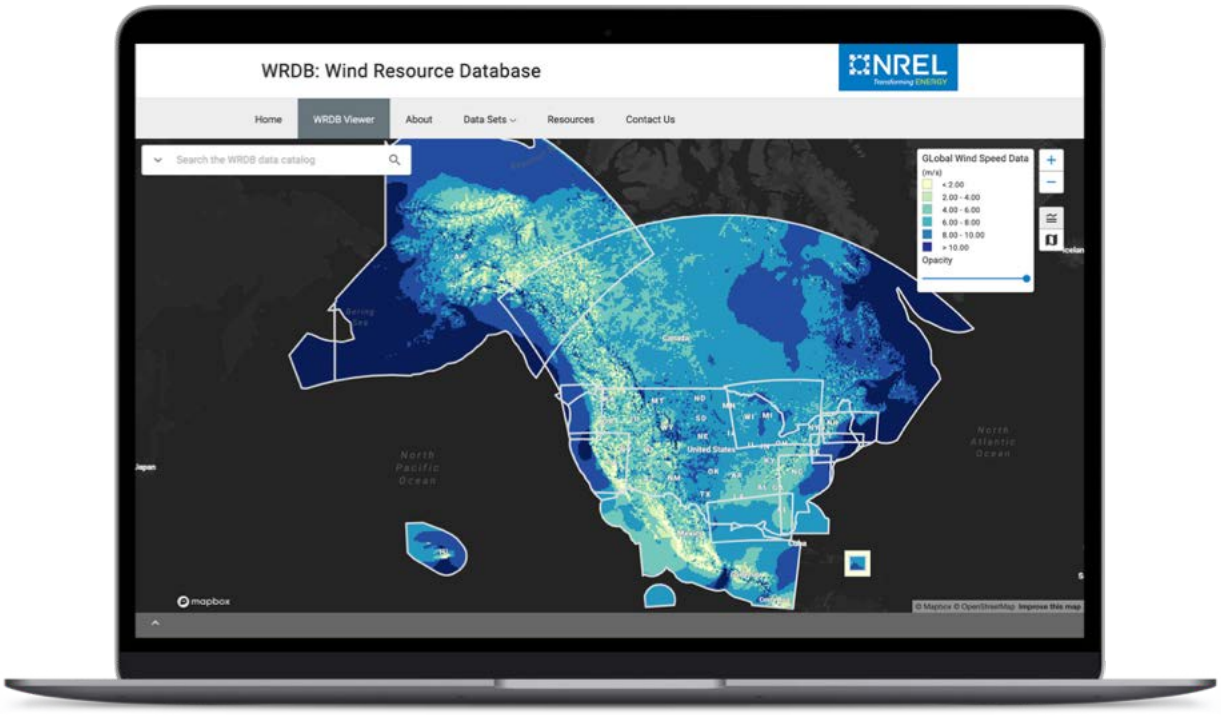

Figure 31. Screenshot of the Wind Resource Database

Table 7. Height and Temporal Resolution for WTK-LED Variables for the North America, CONUS, and Alaska Domains

Variable	Height (m)	Temporal Resolution
Wind speed	10, 20, 40, 60, 80, 100, 120, 140, 160, 180, 200, 250, 300, 500, 1,000	2018–2020: 5 min, 2 km 2000–2020 climate: hourly, 4 km
Wind direction	10, 20, 40, 60, 80, 100, 120, 140, 160, 180, 200, 250, 300, 500, 1,000	2018–2020: 5 min, 2 km 2000–2020 climate: hourly, 4 km
Temperature	2, 20, 40, 60, 80, 100, 200, 300, 500, 1,000	Hourly
Virtual potential temperature	2, 20, 40, 60, 80, 100, 200, 300, 500, 1,000	Hourly
Pressure	0, 100, 200, 500	Hourly
Turbulence kinetic energy*	2, 20, 40, 60, 80, 100, 200, 300, 500, 1,000	2018–2020: 5 min, 2 km
Vertical wind speed*	10, 40, 80, 120, 200, 500	2018–2020: hourly, 2 km
Cumulative precipitation	0	Hourly
Inverse Monin-Obukhov length	2	Hourly
Skin temperature	0	Hourly
Latent heat flux	0	Hourly
Sensible heat flux	0	Hourly
Friction velocity	2	Hourly
Boundary layer height	N/A	Hourly

*Not available for WTK-LED Climate

6 Discussion

The WTK-LED aims to provide valuable data to a wide group of stakeholders across various wind energy disciplines and to address some of the gaps in current publicly available datasets. These gaps include long-term continuity, high spatial and temporal resolution, inclusion of variables relevant to wind energy, and estimates of model uncertainty. The latter is particularly important: The Energy Systems Integration Group (2023) report states, "It should be understood that no model can consistently predict wind speeds to within the 1-2 m/s accuracy range that is needed" for power systems applications, and that "any gridded dataset will be imperfect." By making uncertainty estimates available to the community, users can incorporate these into their analyses and find ways to work around the inherent inaccuracy of modeled data. Acknowledging and embracing model uncertainty is crucial, as errors in hub-height wind speed estimates can have serious financial implications (Veers et al. 2019).

The overall uncertainty of the WTK-LED can only be assessed through rigorous validation and comparison with observations, but those are sparse at hub height. This report includes some validation results, yet we encourage WTK-LED data users to perform additional validation studies based on their needs and required hub heights. For WTK-LED Climate, our results show reasonable outcomes on an aggregated timescale and indicate that for grid integration applications that require hour-to-hour variability, the WTK-LED Climate data should not be used.

Based on our results to date, Table 8 provides recommendations and suggested use cases and applications for each dataset of the WTK-LED.

Table 8. Suggested Use Cases for WTK-LED Datasets. Note that for all datasets a priori validation is strongly recommended.

Dataset	WTK-LED CONUS and WTK-LED Alaska	WTK-LED Climate	NOW-23
Description	Simulations from 2018 to 2020 at 5 min and 2 km resolution	Simulations covering North America from 2001 to 2020 at hourly and 4 km resolution	Simulations at 5 min and 2 km resolution for offshore areas and Hawaii for 20+ years
Use case: wind resource assessments	Preliminary land-based wind resource assessments including interannual, seasonal, diurnal variability assessments	Averaged wind resource estimates (e.g., interannual variability, long-term averaged seasonal and diurnal variabilities); Applications needing high-resolution data covering North America	Preliminary offshore wind resource assessments, including interannual, seasonal, diurnal variability assessments
Use case: grid integration	Land-based grid integration studies	Avoid time-specific grid integration analyses	Offshore grid integration studies

Use case: environmental modeling and airborne wind energy	Environmental modeling (the data include vertical wind speed and turbulence kinetic energy) or airborne wind energy assessments (the data are available up to 1000 m above ground level)	Vertical wind speed and turbulence kinetic energy is not available.	Offshore studies requiring data up to 500 m; vertical wind speed and turbulence kinetic energy not included
Use case: statistical weather analyses	Shorter-term (up to 3-year) statistical analyses	Risk analysis about wind extremes due to natural hazards (hurricanes, wildfire)	Risk analysis about wind extremes due to natural hazards (hurricanes)

In the future, we plan to offer WTK-LED bias correction for locations with sufficient observational coverage. A variety of correction methodologies were assessed using the original WIND Toolkit and reanalysis models to narrow down the best techniques to apply to the WTK-LED in the future. At 10 spatially and temporally diverse observational locations, four computationally inexpensive techniques were tested with the WIND Toolkit: linear scaling, variance scaling, Weibull scaling (Li et al. 2019), and multiplicative ratio (Valappil et al. 2020). Each correction technique was applied according to the following spatiotemporal designations:

1. Bulk: Information is utilized from the entire time period of each surrounding observational contribution, and the results are averaged across the spatial domain prior to application to the bias correction schemes. Temporal coverage can vary between observational location and height.
2. Inverse distance weighted: This correction follows the form of the bulk correction, but instead of averaging the information from the surrounding points, inverse distance weighting is employed so that the surrounding points closest to the central point impact the correction schemes more than distant surrounding points.
3. Vertical nearest neighbor: This correction also follows the form of the bulk correction, but with the restriction of including only the nearest neighbor in vertical height from each surrounding point to the correction height.
4. Seasonal: A unique correction is applied for each season, defined as winter (December, January, February), spring (March, April, May), summer (June, July, August), and fall (September, October, November).
5. Diurnal: A unique correction is applied for different times of day, defined as morning (0600–1159 local time), afternoon (1200–1759 local time), evening (1800–2359 local time), and night (0000–0500 local time).
6. Seasonal + diurnal: Each seasonal definition in conjunction with each diurnal definition is applied, resulting in 16 unique corrections based on time of year and day.

Meteorological tower and airport station data were sourced from Bonneville Power Association, the National Data Buoy Center, the University of Massachusetts, the National Centers for

Environmental Information, and proprietary sources to perform the bias correction assessment (Duplyakin et al. 2021). The computationally inexpensive bias correction assessment showed that linear scaling with any spatiotemporal application and multiplicative ratio scaling applied diurnally reduce the WIND Toolkit bias without degrading the remaining error statistics, namely MAE, RMSE, and R^2. Therefore, the bias correction strategy considered will consider bulk linear scaling and diurnal multiplicative ratio scaling as viable options for bias correcting the WTK-LED in regions with sufficient observational coverage and bias consistency.

Phillips et al. (2022) and Phillips et al. (2024) tested three data-driven bias correction techniques on the KNW-Atlas reanalysis model using observational data from small wind turbines in the Netherlands: multiple linear regression fitted by ordinary least squares, random forest, and support vector regression. Similarly, Sheridan et al. (2024) assessed the performance of multivariable linear regression, adaptive regression splines, and random forest using observations with durations of one year or less. Across the studies, random forest was found to best model the training data in terms of reducing bias, so this method was also selected for consideration in the bias correction strategy.

7 Summary and Conclusions

To satisfy a wide group of stakeholders across various wind energy disciplines and to close some of the gaps that current publicly available datasets have, our team developed an updated version of the original meteorological WIND Toolkit (Draxl et al. 2015a) that now includes the entire United States as well as estimates of model uncertainty of wind speed at every modeling grid point. The updated WIND Toolkit, named WIND Toolkit Long-term Ensemble Dataset (WTK-LED), includes the contiguous United States and Alaska with high-resolution data available for 3 years (2018–2020). Additionally, we leveraged climate simulations from Argonne National Laboratory, which complement the new WTK-LED to offer a 4-km dataset covering 20 years, from 2001 to 2020, covering the North American continent and surrounding oceans, including Alaska, Canada, most of Mexico, and the Caribbean islands. Additionally, specific long-term, high-resolution offshore simulations have been conducted for offshore wind resource assessments in the Atlantic, Great Lakes, Hawaii, Pacific regions, and Gulf of Mexico (NOW-23; Bodini et al. 2024). Because the offshore simulations are documented separately, this report focuses on a description of the land-based WTK-LED for CONUS, Hawaii, and Alaska.

We generated 16 ensemble members to estimate model uncertainty, including internal variability and structural uncertainty, for both summer and winter months. In summary, we found that regardless of the domain size (Alaska vs. North America), summer generally exhibits lower wind speeds while winter shows higher wind speeds. However, summer has higher internal variabilities while winter has lower internal variability. Regardless of the domain size, winter has larger structural uncertainty, which is due to the selected model physics options. We also found that the larger model domain (i.e., North America domain) shows larger internal variabilities as well as structural uncertainties (especially in the summer) (not shown). Comparing the two sources of uncertainty over the same domain and same season, the physics uncertainty is larger than the uncertainty due to model internal variability, but this depends on specific locations. The uncertainty due to internal variability does not change much when using different physics schemes or different forcing data, or in a different year (similar findings can be found in Wang et al. 2018, Lucas-Picher et al. 2008, Braun et al. 2012).

In general, the model uncertainty is much larger for shorter timescales of days or hours and smaller on a monthly scale. We found that the ensemble size required to quantify uncertainty from both interannual variability and structural uncertainty should not be smaller than 12. Most importantly, because the model uncertainty is heavily dependent on the domain size, it has to be quantified for any particular model domain size used for generating wind resource data. Data generated based on one domain size do not have the same uncertainties as the data generated based on another domain size, even when using the same numerical model and model setup.

Simply adding up the uncertainties of structural uncertainty and internal variability is not the best way to express model uncertainty. We developed a resampling strategy and probability distribution functions to quantify the uncertainty of simulated quantities of interest for the AT&T climate risk and resilience project (Gamelin et al. 2022). Therefore, we will make the uncertainties available in the format suggested by Gamelin et al. (2022).

Lastly, the authors would like to reiterate that with any simulated dataset, the value of the dataset increases as more validation is carried out and limitations of the dataset are known. To that end,

we have started to develop recommendations for each of the datasets included in the WTK-LED in Table 8 and will update our guidance as more studies become available. Please contact us for questions and to share results at windtoolkit@nrel.gov.

References

Abraham, Aliza, and Jiarong Hong. 2021. "Operational-Dependent Wind Turbine Wake Impact on Surface Momentum Flux." *Renewable and Sustainable Energy Reviews* 144: 111021. https://doi.org/10.1016/j.rser.2021.111021.

Akinsanola, A. A., C. Jung, J. Wang, and V. R. Kotamarthi. 2024. "Evaluation of precipitation across the contiguous United States, Alaska, and Puerto Rico in multi-decadal convection-permitting simulations." *Scientific Reports*, 14(1), 1238.

Alaska Energy Authority. No date. "Wind Energy Analysis Data - Resource Assessment Data." Accessed December 2023. https://www.akenergyauthority.org/What-We-Do/Renewable-Energy-and-Energy-Efficiency-Programs/Wind/Analysis-Data.

Alexandru, A., R. de Elía, and R. Laprise. 2007. "Internal Variability in Regional Climate Downscaling at the Seasonal Time Scale." *Monthly Weather Review* 135:3221–3238. https://doi.org/10.1175/MWR3456.1.

Amazon Sustainability Data Initiative. No Date. "Amazon's Public Data Initiative." Accessed: Aug. 22, 2024. https://aws.amazon.com/marketplace/pp/prodview-ykfcovxxc4vnw?sr=0-1&ref_=beagle&applicationId=AWSMPContessa#overview.

Andriano, Jennifer R. 2009. "The Power of Wind: Current Legal Issues in Siting for Wind Power." *Planning & Environmental Law* 61(5): 3–13. https://doi.org/10.1080/15480750902963328.

Beiter, Philipp, Jessica Lau, Joshua Novacheck, Qing Yu, Gord Stephen, Jennie Jorgenson, Walter Musial, and Eric Lantz. 2020a. *The Potential Impact of Offshore Wind Energy on a Future Power System in the U.S. Northeast*. Golden, CO: National Renewable Energy Laboratory. NREL/TP-5000-74191. https://www.nrel.gov/docs/fy20osti/74191.pdf.

Beiter, Philipp, Walter Musial, Patrick Duffy, Aubryn Cooperman, Matt Shields, Donna Heimiller, and Mike Optis. 2020b. *The Cost of Floating Offshore Wind Energy in California Between 2019 and 2032*. Golden, CO: National Renewable Energy Laboratory. NREL/TP-5000-77384. https://www.nrel.gov/docs/fy21osti/77384.pdf.

Benton, Brandon N., Grant Buster, Pavlo Pinchuk, Andrew Glaws, Ryan N. King, Galen Maclaurin, and Ilya Chernyakhovskiy. 2024. "Super Resolution for Renewable Energy Resource Data With Wind From Reanalysis Data (Sup3rWind) and Application to Ukraine." Preprint, *ArXiv*, July 26, 2024. https://doi.org/10.48550/arXiv.2407.19086.

Bodini, N., S. Castagneri, and M. Optis. 2023. "Long-Term Uncertainty Quantification in WRF-Modeled Offshore Wind Resource off the US Atlantic Coast." *Wind Energy Science* 8(4): 607–620. https://doi.org/10.5194/wes-8-607-2023.

Bodini, N., M. Optis, S. Redfern, D. Rosencrans, A. Rybchuk, J. K. Lundquist, V. Pronk, et al. 2024. "The 2023 National Offshore Wind Data Set (NOW-23)." *Earth System Science Data* 16(4): 1965–2006. https://doi.org/10.5194/essd-16-1965-2024.

Bodini, N., S. Redfern, A. Rybchuk, V. Pronk, S. Castagneri, A. Purkayastha, C. Draxl, et al. 2023. *NOW-23: The 2023 National Offshore Wind Data Set*. National Offshore Wind Research and Development Consortium. https://nationaloffshorewind.org/wp-content/uploads/147502_Final-Report.pdf.

Bodini, N., A. Rybchuk, M. Optis, W. Musial, J. K. Lundquist, S. Redfern, C. Draxl, R. Krishnamurthy, and B. Gaudet. 2022. *Update on NREL's 2020 Offshore Wind Resource Assessment for the California Pacific Outer Continental Shelf*. Golden CO: National Renewable Energy Laboratory. NREL/TP-5000-83756. https://doi.org/10.2172/1899984.

Boretti, Alberto, and Stefania Castelletto. 2020. "Low-Frequency Wind Energy Variability in the Continental Contiguous United States." Energies 13(1): 144. https://doi.org/10.3390/en13010144.

Braun, M., D. Caya, A. Frigon, and M. Slivitzky. 2012. "Internal Variability of the Canadian RCM's Hydrological Variables at the Basin Scale in Quebec and Labra." *Journal of Hydrometeorolgy* 13(2): 443–462. https://doi.org/10.1175/JHM-D-11-051.1.

Chen, F., and J. Dudhia. 2001. "Coupling an Advanced Land Surface–Hydrology Model With the Penn State–NCAR MM5 Modeling System. Part I: Model Implementation and Sensitivity." *Monthly Weather Review* 129(4): 569–585. https://doi.org/10.1175/1520-0493(2001)129%3C0569:CAALSH%3E2.0.CO;2.

Computational and Information Systems Laboratory. No date. "HPE/SGI ICE XA – Cheyenne" (Wyoming-NCAR Alliance). Boulder, CO: National Center for Atmospheric Research. doi:10.5065/D6RX99HX.

Cox, S., A. Lopez, A. Watson, and N. Grue. 2018. *Renewable Energy Data, Analysis, and Decisions: A Guide for Practitioners*. Golden, CO: National Renewable Energy Laboratory. NREL/TP-6A20-68913. https://www.nrel.gov/docs/fy18osti/68913.pdf.

Douville, Travis C., and Dhruv Bhatnagar. 2021. "Exploring the Grid Value of Offshore Wind Energy in Oregon." *Energies* 14(15): 4435. https://doi.org/10.3390/en14154435.

Draxl, C., A. Clifton, B. M. Hodge, and J. McCaa. 2015a. "The Wind Integration National Dataset (WIND) Toolkit." *Applied Energy* 151: 355–366. https://doi.org/10.1016/j.apenergy.2015.03.121.

Draxl, C., B. M. Hodge, A. Clifton, and J. McCaa. 2015b. *Overview and Meteorological Validation of the Wind Integration National Dataset Toolkit*. Golden, CO: National Renewable Energy Laboratory. NREL/TP-5000-61740. https://www.nrel.gov/docs/fy15osti/61740.pdf.

Duplyakin, D., S. Zisman, C. Phillips, and H. Tinnesand. 2021. *Bias Characterization, Vertical Interpolation, and Horizontal Interpolation for Distributed Wind Siting Using Mesoscale Wind Resource Estimates*. Golden, CO: National Renewable Energy Laboratory. NREL/TP-2C00-78412. https://www.nrel.gov/docs/fy21osti/78412.pdf.

Energy Systems Integration Group. 2023. *Weather Dataset Needs for Planning and Analyzing Modern Power Systems (Summary Report). A Report of the Weather Datasets Project Team*. Reston, VA. https://www.esig.energy/weather-data-for-power-system-planning.

Feng, Cong, Erol Kevin Chartan, Bri-Mathias Hodge, and Jie Zhang. 2017. "Characterizing Time Series Data Diversity for Wind Forecasting." Presented in Proceedings of the Fourth IEEE/ACM International Conference on Big Data Computing, Applications and Technologies (BDCAT '17). New York, NY: Association for Computing Machinery. https://doi.org/10.1145/3148055.3148065.

Feng, Cong, Mucun Sun, Mingjian Cui, Erol Kevin Chartan, Bri-Mathias Hodge, and Jie Zhang. 2019. "Characterizing Forecastability of Wind Sites in the United States." *Renewable Energy* 133: 1352–1365. https://doi.org/10.1016/j.renene.2018.08.085.

Frech, James, Korak Saha, Paige D. Lavin, Huai-Min Zhang, James Reagan, and Brandon Fung. 2024. "A New Gridded Offshore Wind Profile Product for US Coasts Using Machine Learning and Satellite Observations." Preprint, *Wind Energy Science*, July 16, 2024. https://doi.org/10.5194/wes-2024-77.

Gamelin, B., J. Feinstein, J. Wang, J. Bessac, E. Yan, and V. R. Kotamarthi. 2022. "Projected U.S. Drought Extremes Through the Twenty-First Century With Vapor Pressure Deficit." *Scientific Reports* 12: 8615. https://doi.org/10.1038/s41598-022-12516-7.

Gilliam, R. C., and J. E. Pleim. 2010. "Performance Assessment of New Land Surface and Planetary Boundary Layer Physics in the WRF-ARW." *Journal of Applied Meteorology and Climatology* 49(4): 760–774. https://doi.org/10.1175/2009JAMC2126.1.

Giorgi, F., and X. Bi. 2000. "A Study of Internal Variability of Regional Climate Model." *JGR Atmospheres* 105(D24): 29503–29521. https://doi.org/10.1029/2000JD900269.

Giorgi, F., and L. O. Mearns. 1991. "Approaches to the Simulation of Regional Climate Change: A Review." *Review of Geophysics* 29(2): 191–216. https://doi.org/10.1029/90RG02636.

Hamilton, Sofia D., Dev Millstein, Mark Bolinger, Ryan Wiser, and Seongeun Jeong. 2020. "How Does Wind Project Performance Change With Age in the United States?" *Joule* 4(5): 1004–1020. https://doi.org/10.1016/j.joule.2020.04.005.

Han, Z., H. Ueda, and J. An. 2008. "Evaluation and Intercomparison of Meteorological Predictions by Five MM5-PBL Parameterizations in Combination With Three Land-Surface Models." *Atmospheric Environment* 42(2): 233e249. https://doi.org/10.1016/j.atmosenv.2007.09.053.

Harrison-Atlas, Dylan, Andrew Glaws, Ryan N. King, and Eric Lantz. 2024. "Artificial Intelligence-Aided Wind Plant Optimization for Nationwide Evaluation of Land Use and Economic Benefits of Wake Steering." *Nature Energy* 9: 735–749. https://doi.org/10.1038/s41560-024-01516-8.

Hawbecker, Patrick, Sukanta Basu, and Lance Manuel. 2017. "Realistic Simulations of the July 1, 2011 Severe Wind Event Over the Buffalo Ridge Wind Farm." *Wind Energy* 20(11): 1803–1822. https://doi.org/10.1002/we.2122.

Hawkins, E., and R. Sutton. 2011. "The Potential to Narrow Uncertainty in Projections of Regional Precipitation Change." *Climate Dynamics* 37: 407–418. https://doi.org/10.1007/s00382-010-0810-6.

Hersbach, H., B. Bell, P. Berrisford, S. Hirahara, A. Horányi, J. Muñoz-Sabater, J. Nicolas, et al. 2020. "The ERA5 Global Reanalysis." *Quarterly Journal of the Royal Meteorological Society* 146(730): 1999–2049. https://doi.org/10.1002/qj.3803.

Hong, S. Y., and J. J. Lim. 2006. "The WRF Single-Moment 6-Class Microphysics Scheme (WSM6)." *Journal of the Korean Meteorological Society* 42(2): 129–151.

International Renewable Energy Agency. No date. "Global Atlas." Accessed Dec. 28, 2023. https://www.irena.org/Energy-Transition/Project-Facilitation/Renewable-potential-assessment/Global-Atlas.

James, Eric P., Stanley G. Benjamin, and Melinda Marquis. 2018. "Offshore Wind Speed Estimates From a High-Resolution Rapidly Updating Numerical Weather Prediction Model Forecast Dataset." *Wind Energy* 21(4): 264–284. https://doi.org/10.1002/we.2161.

Jung, C., C. Huang, J. Wang, P. Xue, W. Pringle, and V. R.Kotamarthi. 2023. "Influence of SST and Ocean Waves on the Structure and Intensity of Hurricane Henri (2021) Simulation: A Coupled Modeling Study." American Geophysical Union, December 2023, San Francisco, California.

Li, D., J. Feng, Z. Xu, B. Yin, H. Shi, and J. Qi. 2019. "Statistical Bias Correction for Simulated Wind Speeds Over CORDEX-East Asia." *Earth and Space Science* 6(2): 200–211. https://doi.org/10.1029/2018EA000493.

Lo, J. C., Z. L. Yang, and R. A. Pielke Sr. 2008. "Assessment of Three Dynamical Climate Downscaling Methods Using the Weather Research and Forecasting (WRF) Model." *Journal of Geophysical Research* 113(D9): D09112. https://doi.org/10.1029/2007JD009216.

Lopez, Anthony, Trieu Mai, Eric Lantz, Dylan Harrison-Atlas, Travis Williams, and Galen Maclaurin. 2021. "Land Use and Turbine Technology Influences on Wind Potential in the United States." *Energy* 223: 120044. https://doi.org/10.1016/j.energy.2021.120044.

Lucas-Picher, P., D. Caya, R. de Elía, and R. Laprise. 2008. "Investigation of Regional Climate Models' Internal Variability With a Ten-Member Ensemble of 10-Year Simulations Over a Large Domain." *Climate Dynamics* 31: 927–940. https://doi.org/10.1007/s00382-008-0384-8.

Mai, Trieu, Anthony Lopez, Matthew Mowers, and Eric Lantz. 2021. "Interactions of Wind Energy Project Siting, Wind Resource Potential, and the Evolution of the U.S. Power System." *Energy* 223: 119998. https://doi.org/10.1016/j.energy.2021.119998.

Maloney, Patrick, Ping Liu, Qingyu Xu, James D. McCalley, Benjamin F. Hobbs, Sara Daubenberger, Anders Johnson, and Stan Williams. 2019. "Wind Capacity Growth in the Northwest United States: Cooptimized Versus Sequential Generation and Transmission Planning." *Wind Engineering* 43(6): 573–595. https://doi.org/10.1177/0309524X18814966.

McCullough, Ashley, Lillian Bischof, Ronald Alexander, Selorme Agbleze, and Fernando V. Lima. 2024. "Development of an Algorithm To Evaluate the Performance and Economic Feasibility of Expansion of Solar and Wind Power Generation in the Appalachian Region." *International Journal of Energy for a Clean Environment* 25(8): 99–112. https://doi.org/10.1615/InterJEnerCleanEnv.2024051737.

Mellor, G. L., and T. Yamada. 1982. "Development of a Turbulence Closure Model for Geophysical Fluid Problems." *Reviews of Geophysics* 20(4): 851–875. https://doi.org/10.1029/RG020i004p00851.

Millstein, D., S. Jeong, S., A. Ancell, and R. Wiser. 2023. "A Database of Hourly Wind Speed and Modeled Generation for US Wind Plants Based on Three Meteorological Models." *Scientific Data* 10: 883. https://doi.org/10.1038/s41597-023-02804-w.

Morse, Richard, Sarah Salvatore, Joanna H. Slusarewicz, and Daniel S. Cohan. 2022. "Can Wind and Solar Replace Coal in Texas?" *Renewables: Wind, Water, and Solar* 9(1). https://doi.org/10.1186/s40807-022-00069-2.

Nakanishi, M., and H. Niino. 2006. "An Improved Mellor–Yamada Level-3 Model: Its Numerical Stability and Application to a Regional Prediction of Advection Fog." *Boundary-Layer Meteorology* 119: 397–407. https://doi.org/10.1007/s10546-005-9030-8.

Nakanishi, M., and H. Niino. 2009. "Development of an Improved Turbulence Closure Model for the Atmospheric Boundary Layer." *Journal of the Meteorological Society of Japan. Ser. II* 87(5): 895–912. https://doi.org/10.2151/jmsj.87.895.

National Data Buoy Center. No date. Accessed Dec. 28, 2023. https://www.ndbc.noaa.gov/.

National Oceanic and Atmospheric Administration. No date. "The High-Resolution Rapid Refresh (HRRR)." Accessed Dec. 29, 2023. https://rapidrefresh.noaa.gov/hrrr/.

National Renewable Energy Laboratory. No date. "Tools Assessing Performance for Distributed Wind." Accessed May 10, 2024. https://www.nrel.gov/wind/tools-assessing-performance.html.

Nikiéma, O., and R. Laprise. 2011. "Budget Study of the Internal Variability in Ensemble Simulations of the Canadian Regional Climate Model at the Seasonal Scale." *Journal of Geophysical Research: Atmospheres* 116(D16): D16112. https://doi.org/10.1029/2011JD015841.

Niu, G.-Y., Z.-L. Yang, K. E. Mitchell, F. Chen, M. B. Ek, M. Barlage, A. Kumar, et al. 2011. "The Community Noah Land Surface Model With Multiparameterization Options (Noah-MP): 1. Model Description and Evaluation With Local-Scale Measurements." *Journal of Geophysical Research: Atmospheres* 116(D12): D12109. https://doi.org/10.1029/2010JD015139.

Noh, Y., W. G. Cheon, S. Y. Hong, and S. Raasch. 2003. "Improvement of the K-Profile Model for the Planetary Boundary Layer Based on Large Eddy Simulation Data." *Boundary-Layer Meteorology* 107: 401–427. https://doi.org/10.1023/A:1022146015946.

Novacheck, Josh, and Marty Schwarz. 2021. *Evaluating the Grid Impact of Oregon Offshore Wind*. Golden, CO: National Renewable Energy Laboratory. NREL/TP-6A40-81244. https://www.nrel.gov/docs/fy22osti/81244.pdf.

Ortega, Christina, Amin Younes, Mark Severy, Charles Chamberlin, and Arne Jacobson. 2020. "Resource and Load Compatibility Assessment of Wind Energy Offshore of Humboldt County, California." *Energies* 13(21): 5707. https://doi.org/10.3390/en13215707.

Pan, Z., E. Takle, W. Gutowski, and R. Turner. 1999. "Long Simulation of Regional Climate as a Sequence of Short Segments." *Monthly Weather Review* 127(3): 308–321. https://doi.org/10.1175/1520-0493(1999)127%3C0308:LSORCA%3E2.0.CO;2.

Perr-Sauer, J., C. Tripp, M. Optis, and J. King. 2020. "Short-Term Wind Forecasting Using Statistical Models With a Fully Observable Wind Flow." *Journal of Physics: Conference Series* 1452: 012083. https://doi.org/10.1088/1742-6596/1452/1/012083.

Phillips, C., D. Duplyakin, L. Sheridan, J. Ruzekowicz, M. Nelson, D. Fytanidis, R. Linn, R. Kotamarthi, and H. Tinnesand. 2024. "Resource Assessment for Distributed Wind Energy: An Evaluation of Best-Practice Methods in the Continental US." *Journal of Physics: Conference Series* 2767: 092005. https://doi.org/10.1088/1742-6596/2767/9/092005.

Phillips, C., L. M. Sheridan, P. Conry, D. K. Fytanidis, D. Duplyakin, S. Zisman, N. Duboc, et al. 2022. "Evaluation of Obstacle Modelling Approaches for Resource Assessment and Small Wind Turbine Siting: Case Study in the Northern Netherlands." *Wind Energy Science* 7(3): 1153–1169. https://doi.org/10.5194/wes-7-1153-2022.

Pringle, W. J., J. Wang, K. J. Roberts, and V. R. Kotamarthi. 2021. "Projected Changes to Cool-Season Storm Tides in the 21st Century Along the Northeastern United States Coast." *Earth's Future* 9(7), e2020EF001940. https://doi.org/10.1029/2020EF001940.

Pronk, Vincent, Nicola Bodini, Mike Optis, Julie K. Lundquist, Patrick Moriarty, Caroline Draxl, Avi Purkayastha, and Ethan Young. 2022. "Can Reanalysis Products Outperform Mesoscale Numerical Weather Prediction Models in Modeling the Wind Resource in Simple Terrain?" *Wind Energy Science* 7(2): 487–504. https://doi.org/10.5194/wes-7-487-2022.

Qian, J.-H., A. Seth, and S. Zebiak. 2003. "Reinitialized Versus Continuous Simulations for Regional Climate Downscaling." *Monthly Weather Review* 131(11): 2857–2874. https://doi.org/10.1175/1520-0493(2003)131%3C2857:RVCSFR%3E2.0.CO;2.

Rabie, Paul A., Brandi Welch-Acosta, Kristen Nasman, Susan Schumacher, Steve Schueller, and Jeffery Gruver. 2022. "Efficacy and Cost of Acoustic-Informed and Wind Speed-Only Turbine Curtailment To Reduce Bat Fatalities at a Wind Energy Facility in Wisconsin." *PLoS ONE* 17(4): e0266500. https://doi.org/10.1371/journal.pone.0266500.

Rasmussen, R. M., F. Chen, C. Liu, K. Ikeda, A. Prein, J. Kim, T. Schneider, et al. 2023. Four-Kilometer Long-Term Regional Hydroclimate Reanalysis Over the Conterminous United States (CONUS) (ver. 2.0, December 2023): U.S. Geological Survey data release. https://doi.org/10.5066/P9PHPK4F.

Riccobono, Nicholas. 2023. "Riding on Wind's Curtails: How Abundant Wind Energy Can Accelerate Green Hydrogen." Master's thesis, University of Colorado Boulder. https://scholar.colorado.edu/concern/graduate_thesis_or_dissertations/ht24wk80v.

Satkauskas, I., J. Maack, D. Sigler, K. Panda, S. Bhavsar, M. Reynolds, and W. Jones. 2022. "Data and Multistage Optimization for the New Grid." Poster presented at 2022 Exascale Computing Project Annual Meeting, May 2–6. Golden, CO: National Renewable Energy Laboratory. NREL/PO-2C00-82655. https://www.nrel.gov/docs/fy22osti/82655.pdf.

Schleifer, Anna H., Dylan Harrison-Atlas, Wesley J. Cole, and Caitlin A. Murphy. 2023. "Hybrid Renewable Energy Systems: The Value of Storage as a Function of PV-Wind Variability." *Frontiers in Energy Research* 11: 1036183. https://doi.org/10.3389/fenrg.2023.1036183.

Sheridan, Lindsay M., Caleb Phillips, Alice C. Orrell, Larry K. Berg, Heidi Tinnesand, Raj K. Rai, Sagi Zisman, Dmitry Duplyakin, and Julia E. Flaherty. 2022. "Validation of Wind Resource and Energy Production Simulations for Small Wind Turbines in the United States." Wind Energy Science 7(2): 659–676. https://doi.org/10.5194/wes-7-659-2022.

Sheridan, Lindsay M., Dmitry Duplyakin, Caleb Phillips, Heidi Tinnesand, Raj K. Rai, Julia E. Flaherty, and Larry K. Berg. 2024. "Evaluating the Potential of Short-Term Instrument Deployment To Improve Distributed Wind Resource Assessment." Preprint, Wind Energy Science, May 6, 2024. https://doi.org/10.5194/wes-2024-37.

Skamarock, W. C., and J. B. Klemp. 2008. "A Time-Split Non-Hydrostatic Atmospheric Model for Weather Research and Forecasting Applications." *Journal of Computational Physics* 227(7): 3465–3485. https://doi.org/10.1016/j.jcp.2007.01.037.

Smirnova, T. G., J. M. Brown, and S. G. Benjamin. 1997. "Performance of Different Soil Model Configurations in Simulating Ground Surface Temperature and Surface Fluxes." *Monthly Weather Review* 125(8): 1870–1884. https://doi.org/10.1175/1520-0493(1997)125%3C1870:PODSMC%3E2.0.CO;2.

Stahl, Brent, and Lisa Chavarria. 2009. "Wind Energy Laws and Incentives: A Survey of Selected State Rules." Presented at the American Public Power Association–Legal Seminar, Oct. 10–13, 2010, San Francisco, CA. https://sbaustinlaw.com/library-papers/Wind-Energy-Paper.pdf.

Stanley, Andrew P. J., Owen Roberts, Anthony Lopez, Travis Williams, and Aaron Barker. 2022. "Turbine Scale and Siting Considerations in Wind Plant Layout Optimization and Implications for Capacity Density." *Energy Reports* 8: 3507–3525. https://doi.org/10.1016/j.egyr.2022.02.226.

Sun, Mucun, Cong Feng, and Jie Zhang. 2020. "Multi-Distribution Ensemble Probabilistic Wind Power Forecasting." *Renewable Energy* 148: 135–149. https://doi.org/10.1016/j.renene.2019.11.145.

Tobias-Tarsh, L., C. Jung, L. Yan, J. Wang and V. R. Kotamarthi. 2023. "Performance Evaluation of a Dynamically Downscaled, Convection-Permitting Regional Climate Model at Simulating North Atlantic Tropical Cyclones." *American Geophysical Union*, December 2023, San Francisco, California.

Valappil, V., M. Temimi, M. Weston, R. Fonseca, N. Nelli, M. Thota, and K. Kumar. 2020. "Assessing Bias Correction Methods in Support of Operational Weather Forecast in Arid Environment." *Asia-Pacific Journal of Atmospheric Sciences* 56: 333–347. https://doi.org/10.1007/s13143-019-00139-4.

Veers, P., K. Dykes, S. Basu, A. Bianchini, A. Clifton, P. Green, H. Holttinen, et al. 2022. "Grand Challenges: Wind Energy Research Needs for a Global Energy Transition." *Wind Energy Science* 7(6): 2491–2496. https://doi.org/10.5194/wes-7-2491-2022.

Veers, P., K. Dykes, E. Lantz, S. Barth, C. L. Bottasso, O. Carlson, A. Clifton, et al. 2019. "Grand Challenges in the Science of Wind Energy." *Science* 366(6464): eaau2027. https://doi.org/10.1126/science.aau2027.

Wang, J., J. Bessac, V. R. Kotamarthi, E. Constantinescu, and B. Drewniak. 2018. "Internal Variability of a Dynamically Downscaled Climate Over North America." *Climate Dynamics* 50: 4539–4559. https://doi.org/10.1007/s00382-017-3889-1.

Wang, J., and V. R. Kotamarthi. 2015. "High-Resolution Dynamically Downscaled Projections of Precipitation in the Mid and Late 21st Century Over North America." *Earth's Future* 3(7): 268–288. https://doi.org/10.1002/2015EF000304.

Wang, Qin, Carlo B. Martinez-Anido, Hongyu Wu, Anthony R. Florita, and Bri-Mathias Hodge. 2016. "Quantifying the Economic and Grid Reliability Impacts of Improved Wind Power Forecasting." *IEEE Transactions on Sustainable Energy* 7(4): 1525–1537. https://doi.org/10.1109/TSTE.2016.2560628.

Wang, Yi-Hui, Ryan K. Walter, Crow White, Matthew D. Kehrli, and Benjamin Ruttenberg. 2022. "Scenarios for Offshore Wind Power Production for Central California Call Areas." *Wind Energy* 25(1): 23–33. https://doi.org/10.1002/we.2646.

Weber, Jochem, Melinda Marquis, Aubryn Cooperman, Caroline Draxl, Rob Hammond, Jason Jonkman, Alexsandra Lemke, et al. 2021. *Airborne Wind Energy*. Golden, CO: National Renewable Energy Laboratory. NREL/TP-5000-79992. https://www.nrel.gov/docs/fy21osti/79992.pdf.

Wu, Q., J. Bessac, W. Huang, J. Wang., and R. Kotamarthi. 2022. "A Conditional Approach for Joint Estimation in Wind Speed and Direction Under Future Climates." *Advances in Statistical Climatology, Meteorology and Oceanography* 8: 205–224. https://doi.org/10.5194/ascmo-8-205-2022.

Xia, Geng, Caroline Draxl, Michael Optis, and Stephanie Redfern. 2022. "Detecting and Characterizing Simulated Sea Breezes Over the US Northeastern Coast With Implications for Offshore Wind Energy." *Wind Energy Science* 7(2): 815–829. https://doi.org/10.5194/wes-7-815-2022.

Yuan, Qiheng. 2020. "Variability Analysis of Wind and Solar Energy for Optimal Power System Integration." Ph.D. thesis, University of Glasgow. https://theses.gla.ac.uk/id/eprint/81387.

Zobel, Z., J. Wang, D. J. Wuebbles, and V. R. Kotamarthi. 2018. "Evaluations of High-Resolution Dynamically Downscaled Ensembles Over the Contiguous United States." *Climate Dynamics* 50: 863–884. https://doi.org/10.1007/s00382-017-3645-6.

Zuckerman, Gabriel R., Anthony Lopez, Travis Williams, Rebecca Green, and Grant Buster. 2023. *Impacts of Siting Considerations on Offshore Wind Technical Potential in the United States*. Golden, CO: National Renewable Energy Laboratory. NREL/TP-6A20-85088. https://www.nrel.gov/docs/fy23osti/85088.pdf.

Appendix A. WRF Name Lists

A.1 Simulations for CONUS:

```
&time_control
 interval_seconds                = 10800,
 input_from_file                 = .true.,
 history_interval                = 18000000,
 frames_per_outfile              = 1,
 restart                         = .true.,
 restart_interval                = 7200,
 io_form_history                 = 11
 io_form_restart                 = 102
 io_form_input                   = 11
 io_form_boundary                = 11
 auxinput4_inname                = "wrflowinp_d<domain>",
 auxinput4_interval              = 180,
 io_form_auxinput4               = 2,
 auxhist15_interval              = 5,
 frames_per_auxhist15            = 1,
 io_form_auxhist15               = 11,
 iofields_filename               = "myoutfields.txt"
 ignore_iofields_warning         = .true.,
 /

 &domains
 time_step                       = 5,
 max_dom                         = 1,
 e_we                            = 2650,
 e_sn                            = 1950,
 e_vert                          = 61,
 p_top_requested                 = 5000,
 num_metgrid_levels              = 38,
 num_metgrid_soil_levels         = 4,
 dx                              = 2000,
 dy                              = 2000,
 grid_id                         = 1,
 parent_id                       = 0,
 i_parent_start                  = 1,
 j_parent_start                  = 1,
 parent_grid_ratio               = 1,
 parent_time_step_ratio          = 1,
 feedback                        = 0,
 smooth_option                   = 2,
 eta_levels                      = 1.0, 0.998600, 0.996000, 0.994000, 0.992000,
                                   0.990000, 0.987592, 0.984486, 0.980977, 0.977016,
                                   0.972544, 0.967500, 0.961813, 0.955403, 0.948185,
```

```
                    0.940062, 0.930929, 0.920670, 0.909158, 0.896257,
                    0.881820, 0.859633, 0.830162, 0.794019, 0.751945,
                    0.704330, 0.659043, 0.615990, 0.575078, 0.536219,
                    0.499329, 0.464324, 0.431126, 0.399657, 0.369845,
                    0.341616, 0.314904, 0.289641, 0.265763, 0.243210,
                    0.221922, 0.201841, 0.182641, 0.164410, 0.148206,
                    0.132526, 0.117709, 0.104002, 0.091398, 0.079808,
                    0.069150, 0.059351, 0.050340, 0.042054, 0.034434,
                    0.027428, 0.020986, 0.015062, 0.009615, 0.004606,
                    0.0,
&physics
 mp_physics             =  10,
 cu_physics             =  0,
 ra_lw_physics          =  4,
 ra_sw_physics          =  4,
 bl_pbl_physics         =  5,
 sf_sfclay_physics      =  5,
 sf_surface_physics     =  2,
 aer_opt                = 1,
 radt                   = 15,
 swint_opt              = 1,
 bldt                   = 0,
 cudt                   = 5,
 icloud                 = 1,
 num_land_cat           = 21,
 sst_update             = 1,
 sf_urban_physics       = 0,
 surface_input_source   = 1,
 num_soil_layers        = 4,
 /
&dynamics
 w_damping              = 1,
 diff_opt               = 1,
 km_opt                 = 4,
 diff_6th_opt           = 0,
 diff_6th_factor        = 0.12,
 base_temp              = 290.
 damp_opt               = 0,
 zdamp                  = 5000.,
 dampcoef               = 0.2,
 khdif                  = 0,
 kvdif                  = 0,
 non_hydrostatic        = .true.,
 moist_adv_opt          = 1,
 scalar_adv_opt         = 1,
 gwd_opt                = 0,
```

/
&bdy_control
spec_bdy_width = 10,
spec_zone = 1,
relax_zone = 9,
spec_exp = 0.33
specified = .true.,
nested = .false.,
/
&grib2
/
&namelist_quilt
nio_tasks_per_group = 0,
nio_groups = 1,
/

A.2 Simulations for North America (Differences to CONUS Simulations Only):

&time_control
interval_seconds = 21600
restart_interval = 10080,
write_hist_at_0h_rst = .true.
override_restart_timers = .true.
auxinput4_interval = 360
auxhist15_interval = 60,
/
&domains
time_step = 10,
e_we = 2050,
e_sn = 1750,
e_vert = 49
eta_levels = 1.000, 0.998, 0.996, 0.994, 0.992, 0.990, 0.985, 0.980, 0.975, 0.970, 0.965, 0.960, 0.955, 0.950, 0.940, 0.930, 0.920, 0.900, 0.880, 0.860, 0.840, 0.820, 0.800, 0.780, 0.760, 0.740, 0.700, 0.660, 0.620, 0.580, 0.540, 0.510, 0.480, 0.450, 0.420, 0.390, 0.360, 0.330, 0.300, 0.270, 0.240, 0.210, 0.180, 0.150, 0.120, 0.090, 0.060, 0.030, 0.000
dx = 4000,
dy = 4000,
smooth_option = 0
use_adaptive_time_step = .true.,
step_to_output_time = .true.,
target_cfl = 1.2,
target_hcfl = .84,
max_step_increase_pct = 5,
starting_time_step = -1,
max_time_step = -1,
min_time_step = 5,
adaptation_domain = 1,

```
 sfcp_to_sfcp          = .true.
/
 &physics
  bl_pbl_physics                  = 1,
 sf_sfclay_physics                = 1,
 sf_surface_physics               = 2,
 radt                          = 30,
 topo_wind                        = 1,
 /
 &dynamics
 epssm                          = 0.4
 /
 &bdy_control
 spec_exp                        = 0
 /
```

A.3 Simulations for Hawaii (Differences to CONUS Simulations Only):

```
 &time_control
 interval_seconds                 = 3600,
 history_interval                 = 180,  180,
 frames_per_outfile               = 8, 8,
 auxinput4_interval               = 60, 60,
 auxhist15_interval               = 180, 5,
 frames_per_auxhist15               = 8, 1,
 /
 &domains
 time_step                      = 20,
 max_dom                         = 2,
 e_we                           = 309, 727,
 e_sn                           = 283, 649,
 dx                             = 6000,  2000,
 dy                             = 6000,  2000,
 i_parent_start                   = 1,     35,
 j_parent_start                   = 1,     33,
/
&physics
 mp_physics                       =  5,   5,
 cu_physics                       =  1,   0,
 radt                           =  6,   6,
 /

&dynamics
 hybrid_opt                     = 2,
 w_damping                        = 0,
 damp_opt                       = 3,
 zdamp                          = 5000.,  5000.,
```

```
 gwd_opt                             = 1,
 /
 &bdy_control
 spec_bdy_width                      = 5,
 specified                           = .true.
spec_exp                             = 0
 /
 &namelist_quilt
 nio_tasks_per_group                 = 16,
 nio_groups                          = 4,
 /
```

A.4 Simulations for Alaska (Differences to CONUS Simulations Only):

```
 &domains
 e_we                                = 1889,
 e_sn                                = 1419,
 smooth_option                       = 2,
/
&dynamics
 epssm                               = 0.4,
 /
```